

72320 Roversystemtechnik
Summer Semester 2021

INSPIRE

IN-situ Sampling and Primal Investigation Rover on Europa

Phase 0/A-Study of a Rover Mission on the Surface of the Jupiter moon Europa

Denis Acker
Daniel Bölke
Korbinian Kasper
Christian Korn
Nicolas Probst
Saskia Süllerlin

Supervisors:
Moritz Nitz M.Sc.
Patrick Winterhalder M.Sc.

University of Stuttgart
Institute of Space Systems
Prof. Dr. Sabine Klinkner
18.07.2021

Symbols

| Symbol | Definition | Unit |
|------------------------------|---|----------------------|
| a | Constant for the Geometry of a Porous Media | nm |
| A | Wheel Ground Contact Area | m |
| b | Wheel Width | m |
| c | Coefficient of Soil Cohesion | Pa |
| $C_{\text{Batt},\text{req}}$ | Total Required Battery Capacity | Wh |
| $C_{\text{Batt},\text{nom}}$ | Battery Nominal Capacity | Wh |
| C_{cell} | Cell Voltage | V |
| CON_* | Heat conductance of concerning component | $\frac{W}{K}$ |
| C_{rr} | Rolling Resistance Coefficient | - |
| d | Wheel Diameter | m |
| DoD | Depth of Discharge | % |
| DP | Drawbar Pull | N |
| H | Soil Thrust | N |
| h_{Ice} | Ice Crust Surface Thickness on Europa | m |
| k_c | Sinkage Modulus | $\frac{kN}{m^{n+2}}$ |
| k_ϕ | Soil Friction Angle Sinkage Modulus | $\frac{kN}{m^{n+3}}$ |
| l | Ground Contact Length | m |
| R_t | Heat resistance | $\frac{K}{W}$ |
| T_{Surface} | Surface Temperature on Europa | K |
| M | Number of Cells in Parallel | - |
| m_{RTG} | RTG Mass | kg |
| m_w | Weight per Wheel | kg |
| n | Soil Deformation Exponent | - |
| N | Number of Cells in Series | - |
| P_{el} | RTG Electrical Power | W_{el} |
| $P_{\text{el},\text{req}}$ | Required Electrical Power | W_{el} |
| P_{mode} | Demanded Electrical Power per Mode | W_{el} |
| \dot{Q} | Heat flow | W |
| S_0 | Solar constant | $\frac{W}{m^2}$ |
| R_b | Bulldozing Resistance | N |
| R_c | Compaction Resistance | N |
| R_g | Gravitational Resistance | N |
| R_r | Rolling Resistance | N |
| S | Radiation surface | m^2 |
| t_e | Mode Duration | s |
| W_{wheel} | Normal Force per Wheel | N |
| z | Sinkage | m |

SYMBOLS

| | | |
|----------------|---|---------------------|
| α | Absorptivity | - |
| α_{BOL} | BOL Specific Power | $\frac{W_{el}}{kg}$ |
| δ_R | Ecliptic latitude of the rover on Europa | ○ |
| ϵ | Emissivity | - |
| η_{LiIon} | Efficiency of LiIon Cells | - |
| λ | Heat conductivity | $\frac{W}{mK}$ |
| λ_R | Ecliptic longitude of the rover on Europa | ○ |
| ϕ | Friciton Angle | ○ |
| φ | View factor | - |
| ρ_E | Albedo of Europa | - |
| ρ_{Ice} | Inner Encoder Ring Diameter | $\frac{kg}{m^3}$ |
| σ_b | Stefan-Boltzmann constant | $\frac{W}{m^2 K^4}$ |
| θ | Slope Angle | ○ |

Abbreviations

| | |
|---------|---|
| BOL | Begin of Life |
| BOM | Begin of Mission |
| COMM | Communications |
| C&DH | Command & Data Handling |
| CPU | Core Processing Unit |
| DoD | Depth of Discharge |
| EOM | End of Mission |
| EPS | Electrical Power System |
| FEC | Forward Error Correction |
| GPR | Ground Penetrating Radar |
| HGA | High Gain Antenna |
| LGA | Low Gain Antenna |
| 2D | Two Dimensional |
| 3D | Three Dimensional |
| PCDU | Power Control and Distribution Unit |
| PCU | Power Control Unit |
| PDU | Power Distribution and Control Unit |
| IMU | Inertial Measurement Unit |
| IRS | Institute of space Systems at the University of Stuttgart |
| INSPIRE | IN-situ Sampling and Primal Investigation Rover on Europa |
| ESA | European Space Agency |
| MMP | Mean Maximum Pressure |
| MP | Mobility Package |
| NASA | National Aeronautics and Space Administration |
| SPENVIS | SPace ENVironment Information System |
| HPC | High Priority Commands |
| RHU | Radioisotope Heater Unit |
| RTG | Radioisotope Thermoelectric Generator |
| eMMRTG | Enhanced Multi Mission Radioisotope Thermoelectric Generator |
| eSMMRTG | Enhanced and Scaled Multi Mission Radioisotope Thermoelectric Generator (3kg) |
| TID | Total Ionizing Dose |
| TRL | Technology Readiness Level |
| OBC | On-Board Computer |
| S/C | Spacecraft |
| SBC | Single Board Computer |

ABBREVIATIONS

Contents

| | |
|---|-------------|
| Symbols | I |
| Abbreviations | III |
| List of Figures | VII |
| List of Tables | VIII |
| 1 The Mission | 1 |
| 2 Payload | 2 |
| 2.1 Ground RADAR | 2 |
| 2.2 Ice Core Drill | 2 |
| 2.3 Sterovision Camera / Observation / Perception | 2 |
| 2.4 RadHard Solar Arrays | 2 |
| 3 Operation | 4 |
| 3.1 Mission Phases | 4 |
| 3.1.1 Scientific Output | 4 |
| 3.1.2 Rover System Modes | 5 |
| 4 Subsystems | 8 |
| 4.1 Structure and Mechanisms | 8 |
| 4.1.1 Storage Configuration and Rover Deployment | 8 |
| 4.1.2 Exploration Configuration | 8 |
| 4.1.3 Static Analysis | 8 |
| 4.1.4 Mass Budget | 8 |
| 4.2 Locomotion | 9 |
| 4.2.1 Design Drivers for Rover Classification | 9 |
| 4.2.2 System Parameters | 9 |
| 4.2.3 Deployment mechanism | 12 |
| 4.3 Electrical Power System | 12 |
| 4.3.1 EPS Budget and Overview | 12 |
| 4.3.2 Energy Source | 13 |
| 4.3.3 Energy Storage | 14 |
| 4.3.4 EPS Power Control and Distribution | 15 |
| 4.4 Communications and Command & Data-Handling | 16 |
| 4.4.1 Operation Concept | 16 |
| 4.4.2 Communication System | 16 |
| 4.4.3 Command & Data Handling | 17 |
| 4.5 Control and Autonomy | 18 |
| 4.6 Thermal Control System | 19 |
| 4.6.1 Concepts | 19 |
| 4.6.2 Thermal Network | 20 |
| 4.6.3 Analysis | 21 |
| 4.6.4 Results | 21 |
| 4.7 Radiation | 23 |
| 4.7.1 Radiation Protection | 23 |

| | | |
|----------|---|-----------|
| 4.7.2 | Components | 23 |
| 4.7.3 | Improvements | 24 |
| 4.7.4 | Conclusion | 24 |
| 5 | Outlook & Risk Assessment | 25 |
| 5.1 | Risk Assessment | 25 |
| 5.2 | Outlook | 25 |
| | Bibliography | 27 |
| | Appendix | 28 |
| A | Structure and Mechanism | 28 |
| B | Locomotion | 29 |
| B.1 | Locomotion Design Drivers | 29 |
| C | Electrical Power System | 32 |
| D | Communications | 34 |
| D.1 | Link Budget | 34 |
| D.2 | Mission Data Output | 35 |
| D.3 | Communications Trade Off | 36 |
| D.4 | Command & Data Handling Trade Off | 36 |
| E | Thermal Controls System | 44 |
| E.1 | Heat energy eqilibrium | 44 |
| E.2 | Heat conductance | 46 |
| E.3 | Heat switch | 50 |
| E.4 | Rover absorptivity | 51 |
| E.5 | Input Values | 51 |
| F | Radiation | 54 |
| F.1 | Jupiters Radiation Environment | 54 |
| F.2 | Radiation Exposures | 55 |
| F.3 | Improvements | 56 |
| G | Digital Appendix | 58 |

List of Figures

| | | |
|-----|---|----|
| 3.1 | Preliminary Mission Timeline for INSPIRE. | 4 |
| 3.2 | Timeline of a mission day during phase 4 | 4 |
| 4.1 | Wheel sinkage z as a function of the slope angle θ of each configuration with different soil parameters, referred to Figure B.2. | 10 |
| 4.2 | Comparison of the rover's soil thrust versus the motion resistance to exceed, each for the soil parameters of snow in Sweden and heavy clay, referenced to Figure B.2. | 11 |
| 4.3 | Functional Flow Chart Diagram for the EPS Subsystem. | 12 |
| 4.4 | Functional Flow Chart Diagram for the EPS Subsystem. | 13 |
| 4.5 | Carbon-based thermal strap <i>LyNX®</i> | 19 |
| 4.6 | Bi-metallic heat switch, [20]. | 20 |
| 4.7 | Change of the heat switch conductivity R_t over the mean temperature T_M | 20 |
| 4.8 | Thermal network of the rover. | 21 |
| 4.9 | Overview of TIDs within different compartments within the rover. | 24 |
| B.1 | Trade-off of the locomotion movement system. The criteria with the respective weighting factors are shown on the left. On the right side are the respective systems. | 29 |
| B.2 | Soil Parameters | 29 |
| B.3 | Various wheel dimensions respective to the weight. Rows highlighted in red are not considered further for system design due to the limit of 200 g weight per wheel. | 30 |
| B.4 | | 31 |
| B.5 | Parameters for the mean maximum pressure for a wheeled rover. | 31 |
| C.1 | Holistic Power Budget of INPSIRE. | 33 |
| D.1 | Rover to Lander complete downlink budget. | 37 |
| D.2 | Lander to Rover complete uplink budget. | 38 |
| D.3 | Bit Error Rate for different FEC codes | 39 |
| D.4 | Transmitter Trade off for the Communication subsystem. | 40 |
| D.5 | Receiver Trade off for the Communication subsystem. | 41 |
| D.6 | Antenna trade off for the Communication subsystem. | 42 |
| D.7 | OBC trade off for the Command & Data Handling subsystem. | 43 |
| E.1 | Conductance characteristic of heat switch diveded in sections. | 50 |
| E.2 | Bi-metallic heat switch, [20]. | 51 |
| E.3 | Digitalised [17] and calculated heat conduction in comparison. $[0.75\text{em}] \lambda(T) = (1.76 \cdot 10^{-4} \frac{\text{W}}{\text{mK}^4} \cdot T^3 - 2.37 \cdot 10^{-1} \frac{\text{W}}{\text{mK}^3} \cdot T^2 + 79.5 \frac{\text{W}}{\text{mK}^2} \cdot T - 5.55 \cdot 10^3 \frac{\text{W}}{\text{mK}}) \cdot f_r [0.75\text{em}]$ Reduction factor: $f_r = 0.8$ | 53 |
| F.1 | Average trapped proton and electron fluxes on an orbit around earth at 25,000 km, through the outer Van Allen radiation belt, and on Europa's orbit around Jupiter. | 54 |
| F.2 | TID of aluminium, titanium, and the optimised radiation structure shown in Table 4.7 with a weight target of all three structures of 0.5 g/cm^2 over 30 days of exposure on Europa. | 55 |
| F.3 | TID for different compartments as seen in Figure 4.9. The E-Bay is shielded by 4 mm aluminium, 0.415 mm lead, and 0.033 mm iron; the camera compartment by 2 mm aluminium, 0.415 mm lead, and 0.033 mm iron; the chassis by 2 mm aluminium; the electric motors by 1 mm aluminium. | 56 |
| F.4 | TID with 4 mm Al shielding over a mission duration of 30 days | 56 |
| F.5 | TID with 4 mm Al shielding and 1 cm of Water over a mission duration of 30 days | 57 |

List of Tables

| | | |
|------|--|----|
| 2.1 | GPR antenna properties | 2 |
| 3.1 | Expected scientific data output of the INSPIRE mission | 5 |
| 3.2 | Collection of Rover System Modes. [Kommt noch in Anhang] | 7 |
| 4.1 | Fundamental rover design and the respective design drivers. | 9 |
| 4.2 | Configurations for rover classification respective to the wheel width bw , wheel diameter d_w and weight per wheel m_w | 10 |
| 4.3 | Parameters for the scaled eSMMRTG based on the eMMRTG. | 13 |
| 4.4 | Power consumption mode used as design case for the battery sizing. | 14 |
| 4.5 | Key criteria of selected communication components | 17 |
| 4.6 | Temperature results in K of thermal analysis, including a margin of ± 15 K. | 22 |
| 4.7 | Optimal shield structure for an Jupiter mission. [Platzhalter] | 23 |
| 5.1 | Subsystem TRL for risk assessment | 25 |
| B.1 | | 30 |
| C.1 | INSPIRE battery parameters. | 32 |
| D.1 | Transmission link parameters | 34 |
| D.2 | Comparison of transmission times per image (message frame bits included) | 35 |
| D.3 | Transmission time and total data output per tal | 35 |
| E.1 | Definition of heat conductance C between the nodes according to Figure 4.8. | 46 |
| E.2 | Definition of heat conductance $CON = \frac{1}{R}$ between the nodes according to Figure 4.8. | 47 |
| E.3 | Definition of heat conductance $CON = \frac{1}{R}$ between the nodes according to Figure 4.8. | 48 |
| E.4 | Definition of heat conductance $CON = \frac{1}{R}$ between the nodes according to Figure 4.8. | 49 |
| E.5 | Sections and range of the switch characteristic. | 50 |
| E.6 | Toggle temperature and amount of bi-metallic heat switch. | 51 |
| E.7 | Temperatur limits of the rover components. | 52 |
| E.8 | Minimum and maximum of surface emisivity and absorptivity values, [21]. | 52 |
| E.9 | Heat conductivity in $\frac{W}{mK}$ | 52 |
| E.10 | Radiation surface and finishing of components. | 53 |
| F.1 | Used components and the respective radiation tolerance and location | 55 |

Chapter 1

The Mission

During the observation of Jupiter, the Galileo spacecraft did also some flybys of the Jupiter moons, [1]. The scientist gathered data from Europa, which supported the evidence of a thick icy surface. The possibility of liquid water underneath lead astrobiologists to the assumption that extraterrestrial life could exist on Europa, [2]. That is why Europa is - beside Mars - an interesting object of research.

Therefore, the ESA will launch the *JUICE* orbiter in 2022 to investigate Europa in more detail, [3]. But also the NASA is developing *Europa Clipper* to get detailed information. Additionally, they plan a lander for Europa to bring scientific instruments onto the surface. [4] [5].

Under the leadership of Prof. Dr.-Ing. Klinkner, the Institute of Aero Space Systems started within a seminar a feasibility study about a rover system to explore Europa surface, which shall be part of the *TRIPLE* mission. This challenge was given to five student teams in order to develop concepts, construct preliminary designs, perform analysis and make evaluations to meet the mission objectives and fit the mandatory requirements.

This report contain the results of the Phase A study of the rover system IN-SITU SAMPLING AND PRIMAL INVESTIGATION ROVER ON EUROPA (INSPIRE).

Chapter 2

Payload

2.1 Ground RADAR

The Ground Radars main task is the identification of suitable drilling sites. Additionally every radar campaign will contribute to further understanding of the ground composition on Europa.

due to its small dimensions the CRUX GPR is selected . The system is tested for lunar application at 800 MHz resulting in a resolution of 15 cm and a penetration depth of 5 m [CRUX RADAR REF]. The INSPIRE mission makes use of a 1.5 GHz frequency to increase the resolution.

Reduced penetration depths are acceptable since the depth of interest for the ice core sampling is 10 cm.

Additionally high frequencies lead to compact antenna design which is beneficial to the INSPIRE mission due to weight constraints. Based on [Paper & Website reference] a custom patch antenna with the properties in Table 2.1 is proposed.

| Substrate ϵ_r | Width | Length | Height | Mass |
|------------------------|-------|--------|--------|--------|
| 20 | 30 mm | 20 mm | 2 mm | 2,73 g |

Table 2.1: GPR antenna properties

2.2 Ice Core Drill

2.3 Sterovision Camera / Observation / Perception

The INSPIRE rover is equipped with five individual cameras. Two are used as stereo vision cameras on an hight adjustable and rotatable telescope arm on the front side of the rover. This ist used to capture a detailed 3D model of the environment with which sizes and distances can be estimated. The remaining three cameras are used as has-cameras which are necessary to obtain data regarding the nearby environment. All cameras are equipped with radiation hardened lenses to prevent browning of the lenses. The main tasks of the camera system is the provision of scientific data and navigation related data. More details regarding the navigation and autonomy are provided in Section 4.5.

2.4 RadHard Solar Arrays

As a secondary mission goal for INSPIRE a cooperation with the european project RadHard which is led by the german solar array manufacturer Azure Space is intended. They are currently developing a new generation of 4 Junction solar cells with an efficiency of up to 35%. But the main feature of the new solar arrays is their radiation hardness which will be the highest radiation hardness ever designed with an efficiency of $> 3\%$ after $1E15 \text{ cm}^{-2} 1\text{MeV}$ electron irradiation. So the Jupiter environment with its extreme radiation would be the best suitable destination for

a test and evaulation mission of this new technology. Therefore INSPIRE will be equipped with 8 RadHard solar cells with a total surface area of $0.0248m^2$ for a technology demonstration[6].

Chapter 3

Operation

.....

3.1 Mission Phases

For the INSPIRE Mission Phase 0 study five basic mission phases have been defined. Furthermore a sixed optional mission phase after the nominal mission lifetime has been established which will be conducted if the rover is still operational after its nominal lifetime.

- **Phase 0:** Launch and Flight Phase
- **Phase 1:** Entry, Descent and Landing Phase
- **Phase 2:** Deployment Phase
- **Phase 3:** Egress, Comissioning and Early Operation Phase
- **Phase 4:** Mission Operation Phase
- **(Phase 5:** Exceeding Mission Operation Phase)

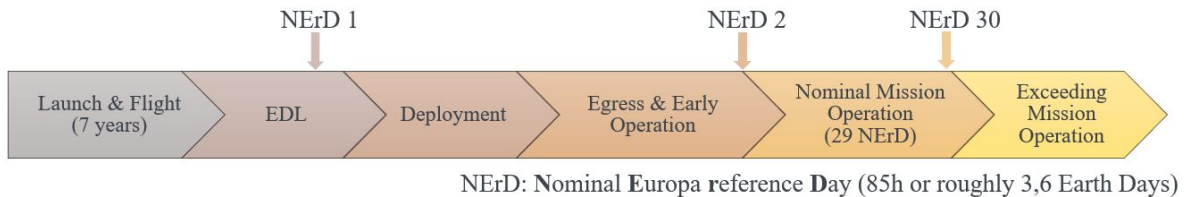


Figure 3.1: Preliminary Mission Timeline for INSPIRE.

Based on these missions phases some preliminary rover system modes as well as a basic mission timeline were concluded.

3.1.1 Scientific Output

Optical reference systems for lath planning limit operation of the rover to an average of 41 h of sunlight. Figure 3.2 depicts a breakdown of the mission day.



Figure 3.2: Timeline of a mission day during phase 4

Locomotion phases consist of a sequence of mobility packages (MP). Each MP is built up of 5 min path planning and 10 s driving. Path planning time is estimated based on the limited

processor speed.

Within the 6 h of a single Locomotion phase, a distance of 64 m is covered, resulting in a maximum distance of 1.6 km for the nominal mission.

With respect to the payloads of the INSPIRE mission described in Chapter 2 the scientific return for Phase 4 will consist of the data in Table 3.1. Out of the 9 h of payload operation a total of 6 h is used for imaging and radar measurements. The total data output can be increased further in the case of a sufficient power margin during operation.

Table 3.1: Expected scientific data output of the INSPIRE mission

| Payload | Data Output | Data Output |
|-----------------|---|-----------------|
| GPR | raw radar measurements | 40 |
| Cameras | grayscale images with optional 3D mapping | >3570 images |
| Sample Analyser | raw mineral analysis of ice core | 10 - 12 samples |
| Solar Cells | performance data | continuous |

3.1.2 Rover System Modes

For this case study several rover system modes were defined. All ten modes are listed in Table 3.2. They are separated into two groups. The design critical modes are displayed in white and are defined as system modes, which significantly influence the preliminary design of the rover subsystem like the thermal or power subsystem. None design critical modes (grey) also have a major influence on multiple subsystems of the rover but play a secondary role in the thermal and power budget of the rover for this Phase 0 study. These non design critical modes extend from the rover storage and launch until the finale deployment of the rover is completed. These modes and their design options depend heavily on the final design of the lander with which INSPIRE flies to Europe. Therefore, a clear definition of such modes is not possible at this time in the course of this phase 0 study. However, the respective considerations, preferences and options have been briefly described in the mode descriptions. It is important to note that INSPIRE's goal is to provide a flexible rover design with as few hard requirements as possible for the parent lander. Therefore, many aspects of the rover, as well as the none design critical modes, will need to be further defined and elaborated in later phases of the project in close consultation with the customer.

For example, the exact interfaces between rover and lander should be defined in more detail. Depending on the subsequently chosen interfaces, many possibilities may arise in the corresponding rover system modes. With an appropriate interface, for example, the excess electrical and thermal energy of the RTG, which is already active during the flight, could be used to supply the lander system with heat and power. A corresponding interface could also enable the transmission of health checks from INSPIRE.

The deployment phase will strongly depend on the final design of the lander, INSPIRE's position within the lander and also the possibilities that the lander provides to INSPIRE. Possible deployment strategies would be as follows:

- **Option 1:** If INSPIRE on ground level: Release from storage box through spring mechanism or actuators. Rover storage configuration allows rolling and possible motorized actuation
- **Option 2:** If INSPIRE is above ground level: Similar as Option 1 but an additional ramp and ramp deployment would be required.

3.1. MISSION PHASES

- **Option 3:** INSPIRE will be deployed through the landers robotic arm if it is capable of lifting its mass.

3.1. MISSION PHASES

| Number | Rover System Modes | Abbreviation | Definition |
|--------|-------------------------------------|--------------|---|
| 0 | Launch/Off Mode | OFF | <p>From Launch until EDL Phase</p> <p>Rover System is OFF</p> <p>Exact mode description t.b.d. and can be adapted to meet the lander demands</p> <p>Health tests on Occasion during flight time are foreseen (PCDU could be active)</p> <p>Batteries on Storage Capacity at launch and may be recharged on occasion (like Rosetta Mission)</p> <p>Telemetry data shall be sent by the Lander (optional if possible)</p> <p>RTG on =>Electrical and Thermal Power may be used</p> <p>(for Lander Power and Thermal Systems) or is disposed of by shunts</p> |
| 1 | Entry, Descent and Landing | EDL | <p>From Entry until next morning after secure landing of Lander on Europa</p> <p>See Mode OFF</p> <p>PCDU ON after secure landing (Powered by RTG)</p> <p>Heaters ON (powered by remaining RTG Power)</p> <p>Battery charging if no Kill Switch is used</p> |
| 2 | Deployment and Early Operation Mode | EOP | <p>First Morning after EDL</p> <p>Exact mode description t.b.d. and can be customized to lander</p> <p>=>Dependant on final Lander Design</p> <p>Critical Deployments (Egress System) and leaving the lander</p> <p>Optional whether Kill Switch ejected =>Battery charging can start</p> <p>Rover System Activation possibilities: Kill Switch, Lander Interface, HPC from Earth</p> <p>PCDU ON</p> <p>OBC ON</p> <p>Heaters ON</p> <p>After sufficient Battery Capacity is reached (50%): Deployment of Rover Boogie and checkout/health check of all Rover Systems</p> <p>Afterward switching to Charging Mode</p> |
| 3 | Idle/ Perception | ID | <p>During Idle Operation Time</p> <p>Rover powered by RTG or Batteries (Excess Power charges Batteries)</p> <p>PCDU ON</p> <p>All Components in Standby or Power Saving Mode if possible</p> <p>Stereovision Camera ON for Orientation and Observation (Science Data)</p> <p>Hazcams and OBC ON for Orientation and Path Analysation</p> <p>COMM ON for larger time intervals (Listening Mode)</p> |
| 4 | Safe Mode/ Hibernation (SAFE) | SAFE | <p>Entered in case of emergency or contingency Rover</p> <p>Survival Mode =>Minimum Power</p> <p>PCDU ON</p> <p>COMM sends Emergency Signal then switches to</p> <p>COMM ON for small time intervals (Listening Mode)</p> <p>OBC OFF until Command received =>High Power Commands (HPC)</p> <p>Heaters ON</p> <p>Science data shall be stored without data loss</p> <p>Applicable during Day and Nighttime</p> <p>Exit after receiving the corresponding command</p> <p>(Optional: Timer ON and Restart of Rover System after time period has passed)</p> |
| 6 | Communication | COMM | <p>During Transmission of major Telemetry or Science Data</p> <p>Rover powered by RTG or Batteries (Excess Power charges Batteries)</p> <p>PCDU ON</p> <p>All Components in Standby or Power Saving Mode if possible</p> <p>OBC SB</p> <p>COMM ON (Transmission Mode)</p> |
| 7 | Charging | BAT | <p>For Battery charging</p> <p>Rover batteries charged by RTG</p> <p>PCDU ON</p> <p>All Components in Standby or Power Saving Mode if possible</p> <p>OBC SB</p> <p>Quit after sufficient charge is reached</p> |
| 8 | Locomotion | LOC | <p>For Rover Movement and Observation</p> <p>Locomotion and Navigation ON</p> <p>Hazcams and Traversing Path Analysis ON</p> <p>OBC ON</p> <p>PCDU ON</p> <p>COMM OFF</p> <p>Stereovision Camera ON for Orientation and Observation (Science Data)</p> <p>Only during Daytime</p> |
| 9 | Payload Observation Mode | OBS | <p>Payload Mode for Science Data Collection during Daytime</p> <p>OBC ON</p> <p>PCDU ON</p> <p>COMM OFF</p> <p>Stereovision Camera ON for Orientation and Observation (Science Data)</p> <p>RADAR ON for Ground Investigation =>Drill Location</p> <p>Only during Daytime</p> |
| 10 | Payload: Ice Core Mode | ICE | <p>Payload Mode for Science Data Collection during Daytime or Nighttime</p> <p>OBC ON</p> <p>PCDU ON</p> <p>COMM OFF</p> <p>Ice Core Drill ON during Ice Core Sample Collection</p> <p>Afterwards Sample will be analysed =>APXS ON</p> |

Table 3.2: Collection of Rover System Modes. [Kommt noch in Anhang]

Chapter 4

Subsystems

In this chapter, the individual subsystems of the rover system will be discussed in more detail.

4.1 Structure and Mechanisms

...

4.1.1 Storage Configuration and Rover Deployment

The Main Characteristics of the Rover Chassi design of INSPIRE focuses on compact storage geometry and low Mass. During the design process its been possible to achieve a reduce of volume in comparison to the first INSPIRE chassi design of about xxxThe geometry data in storage configuration is shown in figure XXX. The storage volume that is required is 131 l. For the Rover Deployment there had been a lot of possible concepts, for example a sky crane, a robotic arm or a ramp. Depending of the reason that there are no further informations about the TRIPLE Lander and that the complexity of such a deployment system shoud be as simple as possible, the decission fell on a ramp where INSPIRE will drive slowly downwards the surface of Europa. A possible concept of the rover deployment is shown in the following figure XXX.

4.1.2 Exploration Configuration

When the deployment is sucessfuly done, INSPIRE has to switch from storage - to exploration configuration. This will be possible with a cogwheel mechanism which will be operated by two Motors (QUELLENVERWEIS). When the wheel forks are horizontal to the ground, the rover is ready for its journey. In order to withstand the potential bumps on the moon's surface, a planetary gear differential is installed which should prevent the rover from tipping over by reflecting the pushing force on the other side of the landing gear to ensure ground contact.

4.1.3 Static Analysis

As part of the design process, it was necessary to perform a static analysis of the chassis. The following load cases were considered: - Stowed configuration inside the TRIPLE lander on Europa - Exploration configuration on the surface of Europa The analysis was created with the computer aided design software "Autodesk Inventor". The results of this analysis are shown in the following figures XXX and XXX.

4.1.4 Mass Budget

An really important part of each space system is the mass budget. Due to the strict mass restriction, it was quite difficult to find a suitable concept that is both light and space-saving. In order to make the design process of INSPIRE more effective, a specially selected preferred maximum mass of the chassis with the mechanisms of 5kg was chosen which could also be adhered to. The following table lists the masses of the individual components of the structure and mechanisms system. A table with all components of the INSPIRE Rover system is stored in Appendix A under Mass Budget.

4.2 Locomotion

The locomotion subsystem deals with the aspect of how the rover moves and the technical design, including the selection of components such as motors or gears. Before the components can be determined, however, it is necessary to consider certain parameters and design drivers. These will be introduced in the following, and the decisions or estimations concerning the rover will be presented.

4.2.1 Design Drivers for Rover Classification

The fundamental rover design can be described by the wheel formula 4x4x4, based on a trade-off, presented in Figure B.1. A more detailed design and the main criteria related to this are summarised in Table 4.1.

Table 4.1: Fundamental rover design and the respective design drivers.

| Wheeled System | 4-Wheels |
|--|---|
| One of the most common types of platform - high level of experience - high TRL | Compared to 2-wheels: - stability can be ensured → important for drilling - MMP decreases |
| Compared to other systems: - analysis quite straightforward - simplification → one of the most critical design drivers | Compared to 6-wheels: - less complex → simplification - mass can be reduced |
| All-Wheel Drive | All-Wheel Actuation |
| - traction can be increased - increase of DP and the slope angle θ | - reduces the risk of slippage on ice |

Furthermore, the normal force on Europa can be calculated to $W = m_{\text{total}} \cdot g_{\text{Europa}} = 39.45 \text{ N}$. Since each wheel is individually driven and controllable, the parameters in the following are designed for one wheel; the normal force per wheel is correspondingly $W_w = 9.8625 \text{ N}$.

4.2.2 System Parameters

Regarding techniques of rover movement, it is crucial to consider the local conditions in which the rover will be operating. The surface of Europa can be assumed to be mainly covered by ice. However, since there are also geysers that transport water to the surface, surface areas may be covered by snow. Though Europa's surface temperature does not exceed 130 K, rather icy, hard-packed snow can be assumed. For this study, a conservative design of the rover is considered, with soil parameters of snow in Sweden as well as heavy clay as a substitute for a hard ice surface; both are listed in Figure B.2. Furthermore, the parameters depend on the width and diameter of the wheels of the rover. Therefore, several sizes dependent on the respective weight were selected and a limit per wheel was set to 200 g, illustrated in Figure B.3. This constraint results in 6 configurations considered for the Rover system design, listed in Table 4.2.

Trafficability Configuration

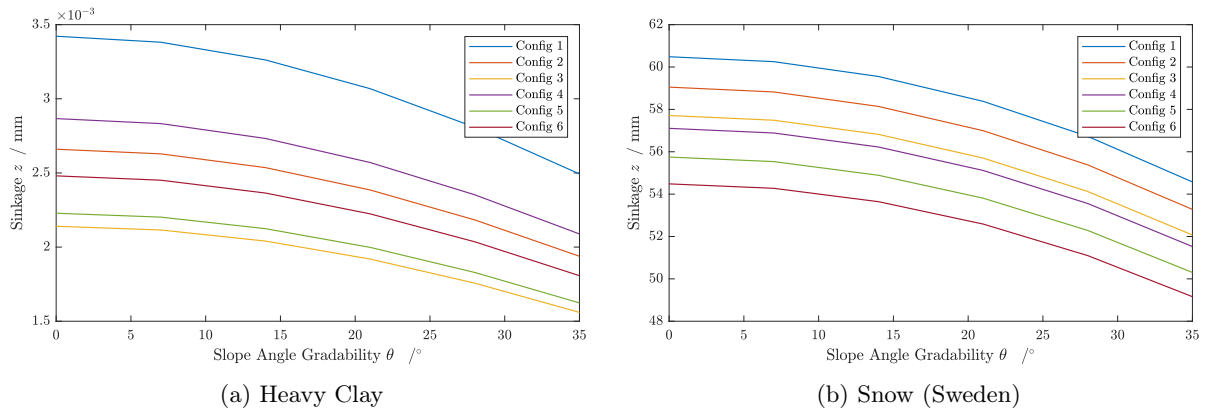
The ability of traffic depends on the soil parameters as well as on the geometric dimensions of the wheels. The sinking depth z for each wheel of the rover can be determined to:

$$z = \left(\frac{3W_{\text{wheel}} \cos \theta}{(3-n)(k_c + b_w k_\phi) \sqrt{d_w}} \right)^{\frac{2}{2n+1}}. \quad (4.1)$$

Table 4.2: Configurations for rover classification respective to the wheel width b_w , wheel diameter d_w and weight per wheel m_w .

| Configuration | b_w /m | Diameter d_w /m | Weight m_w /kg |
|---------------|----------|-------------------|------------------|
| 1 | 0.05 | 0.1 | 0.127 |
| 2 | 0.06 | 0.1 | 0.153 |
| 3 | 0.07 | 0.1 | 0.178 |
| 4 | 0.05 | 0.125 | 0.154 |
| 5 | 0.05 | 0.125 | 0.185 |
| 6 | 0.05 | 0.15 | 0.185 |

As shown in Figure 4.1, the sinking depth z depends not only on the geometric conditions and soil parameters but also on the slope angle θ . Therefore, z can be determined for both soils with respect to θ as plotted in Figure 4.1. However, it can be assumed that for the expected soil, the following applies: $z_{\text{Heavy Clay}} \leq z_{\text{Europa}} \leq z_{\text{Snow}}$.


 Figure 4.1: Wheel sinkage z as a function of the slope angle θ of each configuration with different soil parameters, referred to Figure B.2.

The required power for the rover can be calculated by the resistances that have to be exceeded. For the total resistance, the following applies:

$$R_{\text{total}} = \underbrace{R_{\text{compaction}}}_{= \frac{z^{n+1}}{n+1} (k_c + b k_\phi)} + \underbrace{R_{\text{rolling}}}_{R_r = W_w C_{rr}} + \underbrace{R_{\text{gravity}}}_{R_g = W_w \sin \theta} + \underbrace{R_{\text{bulldozing}}}_{R_b \rightarrow 0}. \quad (4.2)$$

Due to the hard surface of Europa, it can be assumed that $R_b \rightarrow 0$. In contrast to the R_g , R_r can be defined as constant. With a rolling resistance coefficient of $C_{rr} = 0.02$, the resulting resistance is $R_r = 0.1972$ N [rolling coefficient]. Analogous to z , the lower limit of R_{total} with soil properties of heavy clay is plotted in Figure 4.2c, while the upper limit is shown in Figure 4.2d for snow.

In addition to the resistance that needs to be exceeded in order to move, an upper limit can also be determined. The ground thrust H indicates the maximum amount of traction that can be achieved before the wheels slip. Therefore, following applies:

$$H = A \cdot c + W_w \cdot \tan \Phi, \quad (4.3)$$

with the wheel ground contact area $A = \frac{\pi}{4} \cdot b_w \cdot l$ and the ground contact length $l = \frac{d_w}{2}$.

$\cos^{-1} \left(1 - \left(\frac{2z}{d_w} \right) \right)$. As a result, the absolute upper limit of traction is presented in Figure 4.2a for heavy clay and Figure 4.2b for snow.

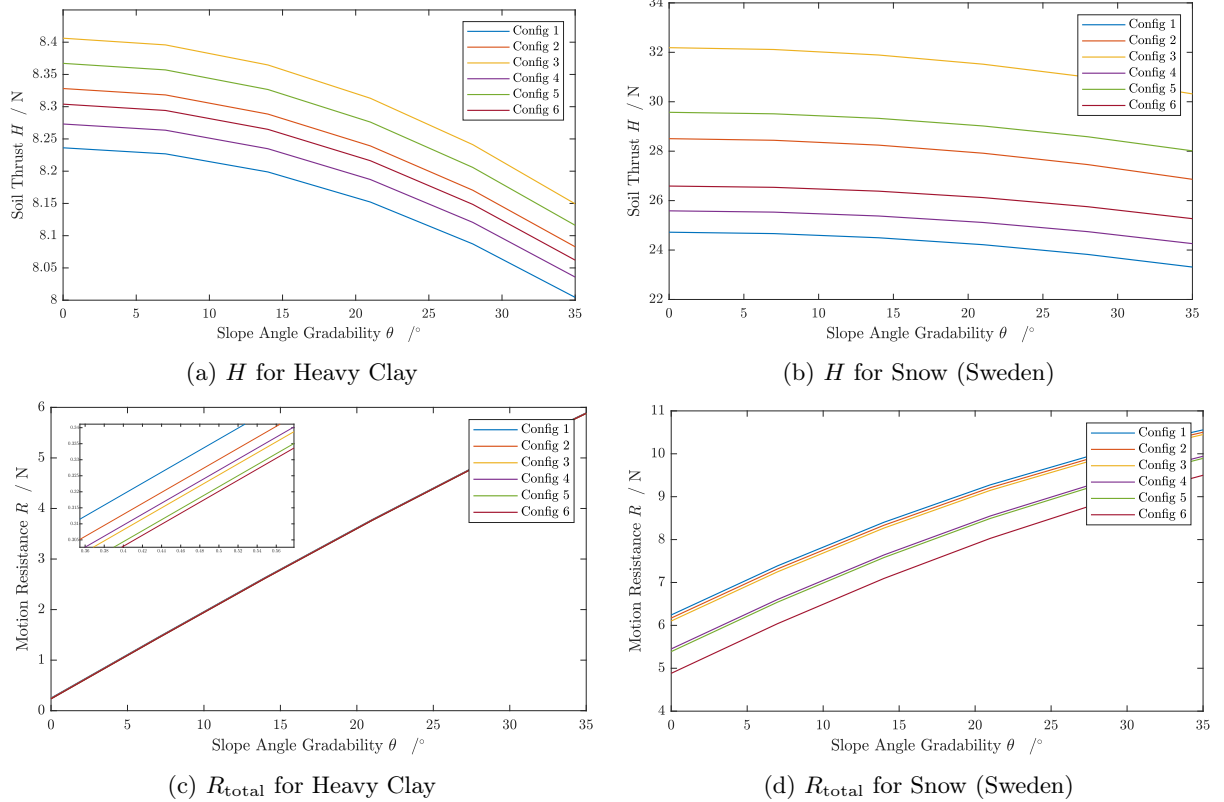


Figure 4.2: Comparison of the rover’s soil thrust versus the motion resistance to exceed, each for the soil parameters of snow in Sweden and heavy clay, referenced to Figure B.2.

In addition to the determined parameters, it should also be verified that the mean maximum pressure MMP does not increase excessively due to the selected geometric parameters. For this conservative calculation, a rigid wheel is assumed, whereby for the deflection δ applies, that $0 \leq \delta \leq 0.1d$. For terrestrial snow, 40 kPa should not be exceeded, but ideally the MMP should be less than 10 kPa. The associated verification calculation can be found in Appendix B.1. For the Rover, configuration 6 is chosen as it offers the lowest resistance to exceed whilst maintaining the lowest MMP .

Steering

Since the rover has an all-wheel actuation, it can be operated with on-point steering and, in order to avoid greater obstacles, with Ackerman steering. Considering that with Ackerman steering, the radius of the outer wheels is at a greater distance in the circumventing circle than that of the inner wheels, the following applies:

$$\cot \theta_i - \cot \theta_o = -\frac{d}{l}. \quad (4.4)$$

With a wheel distance of $d = 277$ mm and $l = 365$ mm, this results in the table shown in Table B.1.

Hardware Selection

For the drive of the wheels, BLDC motors were chosen. In contrast to stepper motors, these are optimised for a uniform torque and not for precise motion control. The resulting torque of each wheel can be calculated to:

$$\tau = R_{\text{total}} \cdot \left(\frac{d_{\text{textw}}}{2} - \delta \right). \quad (4.5)$$

The required power is then resulting in:

$$P = \tau \cdot \left(\frac{2v_{\max}}{d_{\text{textw}}} \right), \quad (4.6)$$

with the estimated maximum velocity v_{\max} .

4.2.3 Deployment mechanism

4.3 Electrical Power System

The EPS (Electrical Power System) is the subsystem responsible for the electrical power supply of INSPIRE. It consists of four fundamental parts, which are the energy source, the PCDU unit (Power Control and Distribution) and the Energy Storage as well as the rover subsystems as the consumers. The EPS is visualized in Figure 4.3.

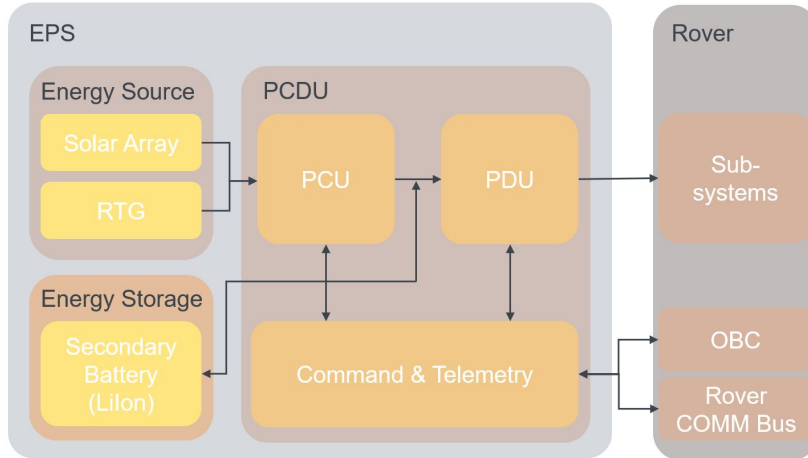


Figure 4.3: Functional Flow Chart Diagram for the EPS Subsystem.

4.3.1 EPS Budget and Overview

Figure 4.4 summarizes the power budget of INSPIRE based on the rover system modes defined in Subsection 3.1.2. The holistic power budget can be found in Figure C.1. As can be seen, the Locomotion mode has the highest demands on the EPS. The two payload modes also have a high power demand. The Communication mode also has a high consumption. However, since this is primarily used at night and the rover can be charged again afterwards without any problems, it does not place any major restrictions on the power budget. Idle/Perception mode has a low consumption, but is usually used for a long time at a stretch and therefore also places high demands on the EPS. In Charging mode, the EPS is able to charge 8.82 W_{el} .

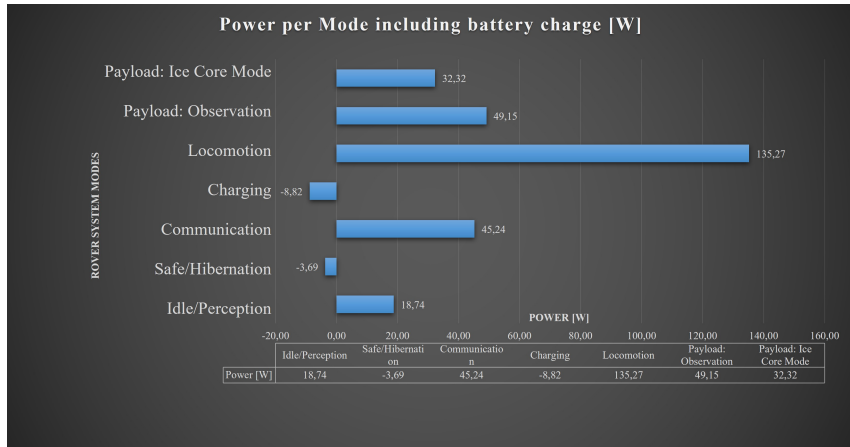


Figure 4.4: Functional Flow Chart Diagram for the EPS Subsystem.

4.3.2 Energy Source

For the energy generation of INSPIRE many possible sources were taken into consideration for a trade-off. As a conclusion of this trade-off the decision was made to utilize a Radioisotope Thermoelectric Generator (RTG) as the main energy source for INSPIRE.

As the research couldn't find an RTG with a mass suitable for INSPIRE, the solution was to scale down a bigger RTG as an approximation. As a baseline of the scaling the eMMRTG (Enhanced Multi Mission Radioisotope Thermoelectric Generator) was utilized, which is currently under development at NASA and is especially designed for deep space missions like Europa. For the scaling a goal RTG mass of $m_{RTG} = 3 \text{ kg}$ was defined and the eMMRTG was scaled down using the given data.

In Table 4.3 the scaling results for the eSMMRTG (Enhanced and Scaled Multi Mission Radioisotope Thermoelectric Generator) are listed. The eSMMRTG has a BOL specific power of $\alpha_{BOL} = 4.0 \frac{W_{el}}{kg}$ and provides an electrical power of $P_{el} = 12.08 \text{ W}_{el}$ during the mission duration[7][8][9][10][11].

Table 4.3: Parameters for the scaled eSMMRTG based on the eMMRTG.

| Scaled eSMMRTG Parameter | |
|--|--------------|
| System Mass m_{RTG} [kg] | 3.5 |
| BOL Specific Power $\alpha_{BOL} \frac{W_{el}}{kg}$ | 4.0 |
| BOL Power $P_{el,BOL} W_{el}$ | 14 |
| Isotrop | Pu-238 |
| Isotrop Half-Life [a] | 87.7 |
| Flight time and Storage (incl. Margins) [a] | 7 |
| Power Loss Degradation until BOM W_{el} | 0.56 |
| BOM Power $P_{el,BOM} W_{el}$ | 13.44 |
| Europa Day Duration [h] | 85 |
| Mission Duration [d] | 106.25 |
| End of Mission Power $P_{el,EOM} [W_{el}]$ | 13.42 |
| Final Power for Study $P_{el} [W_{el}]$ (incl. 10% scaling Margin) | 12.08 |

Furthermore INSPIRE will also be equipped with some radiation hardend solar arrays as already

explained in Section 2.4[6]. Since these solar cells are primarily used for technology testing, the mission must also be able to operate completely without this generated energy. For this reason, and because the expected energy generated by the solar cells is minimal, only the energy generated by the RTG is considered for the Phase 0 Study. However, it should be noted that these solar cells will also generate a certain amount of energy, which will benefit the EPS.

4.3.3 Energy Storage

For the energy storage of INSPIRE many possible battery types were taken into consideration for a trade-off. As a conclusion of this trade-off the decision was made to utilize LiIon batteries as the secondary batteries of INSPIRE. This decision is primarily based on LiIon batteries high energy density, temperature range, robust performance and long operating and cycle life in extreme environments[12]

As the RTG only generates a small constant power the main energy source during the mission will be the accumulated energy of the batteries. The rover will charge the batteries at night, so the next exploration day can start with full capacity. Furthermore the batteries have to be charged during day time to maintain operations.

For the sizing of the batteries, the rover motion was chosen as the design driver, since this is the highest energy consuming state of the rover and additionally mission critical for INSPIRE. The rover motion consists of an interaction of the Locomotion and Perception mode as already mentioned in Chapter 3. Therefore it was defined that INSPIRE shall be able to drive 50 m (including alternating Locomotion and Perception Mode) with a fully charged Battery. Furthermore the battery mass shall not exceed 2 kg. The required battery capacity $C_{\text{Batt},\text{req}}$ can be calculated using Equation 4.7. The results are listed in Table 4.4 [13].

$$C_{\text{Batt},\text{req}} = \frac{P_{\text{el},\text{req}} \cdot t_e}{DoD \cdot \eta_{\text{LiIon}}} \quad (4.7)$$

Table 4.4: Power consumption mode used as design case for the battery sizing.

| Power Consumption Mode: | Locomotion | Perception |
|---|---------------|------------|
| Required Electrical Power $P_{\text{el},\text{req}}$ [W _{el}] | 135.27 | 18.74 |
| Duration of the mode t_e [s] | 500 | 15000 |
| DOD for Dimensioning [-] | 0.90 | 0.90 |
| Efficiency of LiIon Cells η_{LiIon} [-] | 0.95 | 0.95 |
| Required Battery Capacity per mode C_{mode} [Wh] | 21.97 | 91.33 |
| Total Required Battery Capacity $C_{\text{Batt},\text{req}}$ [Wh] | 113.30 | |

Using these values a suitable battery cell and battery design configuration were conducted. Under consideration of these parameters the battery capacity C_{Batt} can be calculated:

$$C_{\text{Batt}} = C_{\text{cell}} \cdot V_{\text{cell}} \cdot N \cdot M. \quad (4.8)$$

According to the ECSS reliability restrictions 1 battery string must be subtracted for dimensioning. Furthermore a 30% margin on the energy content was applied. This leads to a final battery configuration with a capacity of $C_{\text{Batt}} = 156.24$ Wh and a mass of $m_{\text{Batt}} = 1980$ g. The final battery values are listed in Table C.1 [14].

4.3.4 EPS Power Control and Distribution

In order to ensure the full functionality of the EPS, the last main component to be selected is a suitable PCDU. As described in Figure 4.3, the PCDU forms the heart of the EPS and is an important interface to the OBC and COMM. Furthermore the PCDU shall be able to monitor and control the rover system if necessary through watchdogs, HPC (High Priority Commands) and direct connections to the OBC and COMM.

The PCDU has the challenging task not only to process the RTG as the main energy source, but also to process solar cells as secondary energy sources. Therefore, a PCDU was sought which has the required size, dimensions and range of functions. The research resulted in the Nova PCDU from Bradford DSI. In addition, margins were added to the PCDU to ensure feasibility[15].

4.4 Communications and Command & Data-Handling

The Communications subsystem consists of redundant transmitters and receivers which are cross linked to four antennas and the OBC. Additionally hard wired connections to the PCDU enable for reboots via direct commands.

C&DH is responsible for the generation of telemetry from the housekeeping boards and the execution of telecommands, as well as the storing and compressing of payload data.

4.4.1 Operation Concept

Due to power and time constraints, the rover will only transmit telemetry during the locomotion and payload phases. Payload data will be compressed and stored and forwarded to the Lander at the end of a mission tal.

To achieve the scientific output from Subsection 3.1.1 the transmission time per tal is calculated in Subsection D.2 (Table D.3) and adds up to 38,23 minutes.

4.4.2 Communication System

Requiring too many resources a direct link to earth has been deemed impractical. Instead communication for the INSPIRE mission is proposed to rely on a link between the rover and the Europa Lander. The lander then forwards data to earth via a satellite relay carrier which orbits the moon. The lander offers a 25 dB high gain antenna [Missing Reference] and a low gain antenna which is not further specified in literature.

The downlink from the rover to the lander has been identified as the critical transmission path. However, link budget considerations in Subsection D.1 reveal that a transmission to the LGA of the Europa Lander produces a link margin of 10,59 dB, resulting in a Bit Error Rate of less than 10^{-4} . The link budget has been performed under the conservative considerations listed in Table D.1.

Using the Landers LGA greatly increases robustness due to the elimination of pointing errors and higher margin for rover positioning error. Additionally, the INSPIRE rover's communication link would not interfere with the Landers communication to the relay carrier by blocking the HGA.

Component Selection

Due to the considerably high link margin the focus is on low mass and low power components with flight heritage such as flown on CubeSat missions. Criteria with relatively small impact on the link budget such as component noise or even FEC have not been taken into account. Ideally the rover communication uses X-Band for increased compatibility with the lander and has a total system mass of less than 1 kg.

Since radiation hardness was not included in most datasheets a total dose of $< 20 \text{ krad}$ was assumed in accordance with values for LEO [Missing Reference].

The selected components are listed in Table 4.5.

Expected transmission times per mission day are less than 40 minutes (see Subsection D.2 Table D.3). Therefore the transmitter mass is identified as more critical than power.

Receiver duty cycles on the other hand range close to 100 % (REFERENCE POWER BUDGET). Thus power has been identified as the most crucial criteria.

Table 4.5: Key criteria of selected communication components

| Component | Supplier | Part Description | 1. Criteria | Value | 2. Criteria | Value |
|-------------|-----------|------------------|-------------|----------|-------------|-----------|
| Transmitter | Sputnix | SXC-XTX-01 | mass | 0,195 kg | data rate | 10 Mbit/s |
| Receiver | Endurosat | S-Band receiver | power | max. 2 W | mass | 0,220 kg |
| Antenna | Endurosat | patch antenna | mass | 2,2 g | frequency | X-Band |

A passive X-Band antenna was selected due to compact dimensions and no power consumption. The entire trade off can be found in (APP Trade off).

4.4.3 Command & Data Handling

With respect to restricted power supply a redundant OBC hot-cold configuration stands to reason. Additionally, the standby mode is suggested during hibernation and charging modes relying solely on the PCDU (see chapter [Missing Reference]). Emphasis for the Electronics selection is placed on flight proven radiation hardness to increase mission robustness in the high radiation environment of the Jupiter system. Criteria of less importance are CPU speed and dimensions.

Instead of designing a new OBC board a trade-off was performed among existing single board computers. SBCs provide peripheral services such as bus interfaces, timer and memory in a flight proven configuration, which promises an effective mission development.

BAE Systems provides a SBC with their flight proven Power PC750 Architecture which withstands a total radiation dose of up to 1 *Mrad*. The robustness comes at the cost of a 182 *MHz* processor speed.

Additionally a custom housekeeping board will be tasked with providing engine control peripherals and sensor read out electronics.

4.5 Control and Autonomy

4.6 Thermal Control System

The main object of the Thermal Control System (TCS) is to keep the eletric components within their temperature limits, listed in Table E.7. As a result of Europas low surface temperature, a small solar constant and the thin atmosphere the heat loss of the rover has to be minimised [16]. This shall be reached by a smart heat distribution as well as by an adequate insulation and surface finishing.

4.6.1 Concepts

The main heat source of the rover is the waste heat of the RTG (see Section 4.3), which will be lead by thermal straps to the thermperature sensetive components. The first attempt to use straps made out of copper was rejected du to the high resulting mass. Therefore, carbon-based straps *LyNX®* with a high thermal conductivity to density ratio will be used, [17]. However, the thermal conductivity is highly depend on the materials temperature, see Figure 4.5. The curve was approximated by an cubic interpolation, . To consider heat loss as a result of surface contact and radiation, the thermal conductivity was reduced about 20% ($f_r = 0.8$).

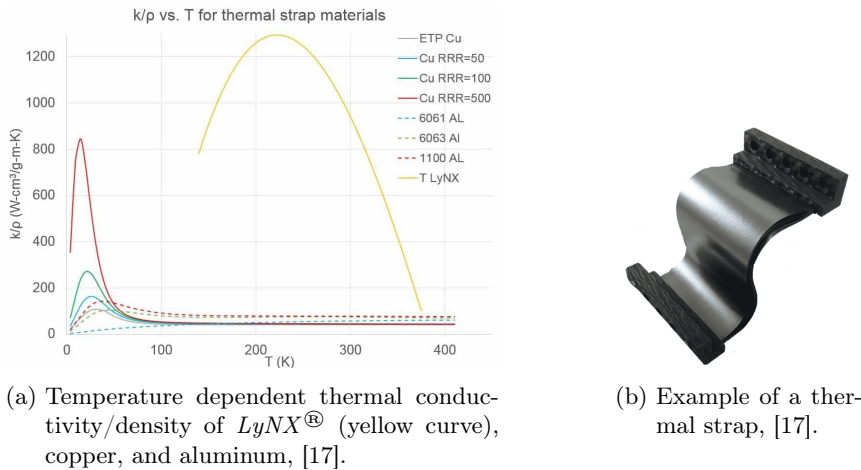


Figure 4.5: Carbon-based thermal strap *LyNX®*.

The camera, exposed on a mast, will be heated by a seperate, light weight Radioisotope Heater Unit (RHU), which has been used during several NASA missions [18]. For the insulation, the material *Aerogel* will be applied, which has a very low heat conductivity ($0.016 - 0.03 \frac{W}{mK}$) as well as a low density ($5 - 200 \frac{kg}{m^3}$) and has also been used in space applications [19].

A surface finishing with an low emisivity for low heat emisivity is necessary. For the most componets, a cost-efficient surface polishing is applicable. The camera will get a special white paint with a high absorptivity to gather the sun light.

But there is also a risk of overheating, because of the lack of heat convection. This circumstance concern the engines and also the camera. To get rid of the extensive heat and to prevent damage of the components special bi-metallic heat switches (see Figure 4.6) will be placed between the application and the connection interface. These switches change their heat conductivity beyond a certain temperatur due to the expansion of the disk (see Figure 4.7a). It was assumed, that the toggle temperatur can be adapted by increasing the disk height. The influence of the changed disk stiffens on the contact pressure and therefore the heat conductivity was neglected for this study. The measured heat conductivity characterisitc was divided in three linear sections (Figure 4.7b), to enable a simple modelling in the upcoming thermal calculation.

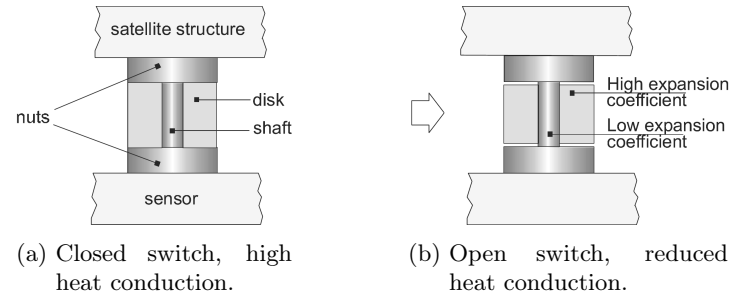
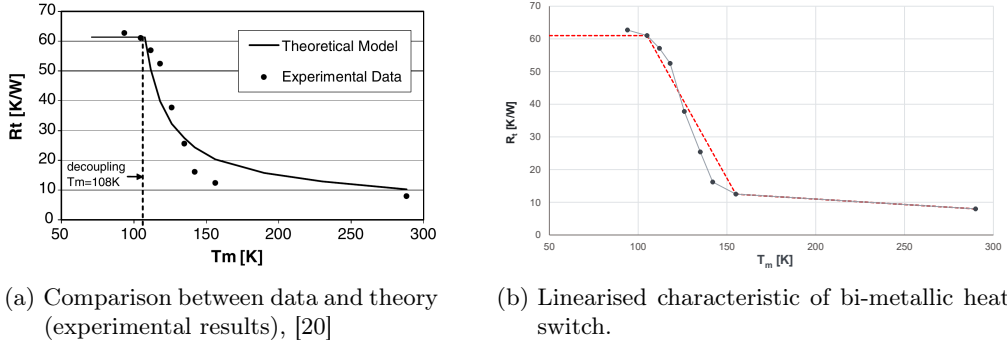


Figure 4.6: Bi-metallic heat switch, [20].


 Figure 4.7: Change of the heat switch conductivity R_t over the mean temperature T_M .

4.6.2 Thermal Network

A thermal analysis was performed in order to get

- the dimension of the insulation and heat straps,
- the necessary amount of RHUs and heat switches,
- the required surface finishing and
- the suitable choice of material.

For that, a thermal network with ten nodes was derived from the rover, shown in Figure 4.8. At the intersection of the steering and drive engien, two additional nodes were defined to calculate the heat flow.

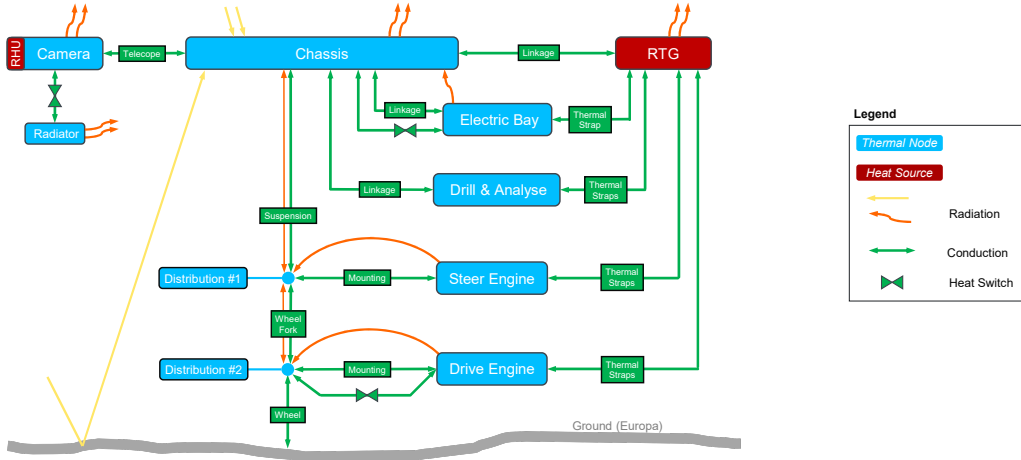


Figure 4.8: Thermal network of the rover.

On the basis of the thermal network, the heat energy equilibrium for each node was defined (see Subsection E.1). The calculation were considered as a quasi-static analysis, were the component temperatures stay constant, $\frac{dT}{dt} = 0$. Due to the early state of the rover, simplifications and assumptions for the analysis were made.

- The convection was neglected due to the thin atmosphere.
- The whole electrical power of the components will be dissipated into heat.
- A variation of $\pm 20\%$ for the emisivity and absorpsivity values was considered, if applicable (see Table E.8).
- The heat as a result of retardation radiation inside the shielding was neglected.
- No discrete nodes for the radar, hazcams and deployment engines were considered. Their heat will be lead into the chassis.

4.6.3 Analysis

The thermal analysis was performed as an Excel calculation, which can be found in the corresponding folder of Team 3. The calculation sheet offers the possibility to adapt and customise input values and dimension. The major driving load cases are the hot and the cold cases, where the maximum and minimum temperatures of the rover components will be reached. For that, the most powerful components were set to operating mode at once or only the minimum required components were turned on, respectively. The emisivity and absorptivity were adjusted to fulfil the cases. There were further load cases defined in order to cover important mission cases.

4.6.4 Results

The resulting temperatures for each node for the hot and cold cases are listed in Table 4.6. The temperature margins for uncertainties, acceptance tests and qualification tests were considered with 5 K each, ± 15 K in total. The corresponding temperatures are listed in Table 4.6. All temperature lay between their limits without using a heater. Nevertheless, heaters were considered for the power calculation, see Section 4.3.

In a further step, a more detailed analysis should be carried out with the Finite-Element-Method to identify the correct heat and temperature distribution. The FE results could be used to verify and adjust the analytical analysis to get a helpful tool for fast thermal calculation to evaluate different materials or designs in the further development phases.

Table 4.6: Temperature results in K of thermal analysis, including a margin of ± 15 K.

| Components | Load Case | | | |
|------------------|-----------|-------|-----------|-------|
| | Hot case | | Cold case | |
| | 0 K | +15 K | 0 K | -15 K |
| RTG | 380 | 395 | 350 | 335 |
| Electric Bay | 310 | 325 | 261 | 246 |
| Drill & Analyser | | | | |
| Camera | | | | |
| Steering Engine | | | | |
| Drive Engine | | | | |

4.7 Radiation

Compared to the radiation environment near Earth the radiation environment near Jupiter is multiple times stronger. It has the highest radiation levels of any planet in our solar systems [Platzhalter]. In order to survive these harsh environmental conditions, special emphasis must be placed on the radiation protection. In Figure F.1, the average trapped proton and electron fluxes on Europa's orbit around Jupiter are shown in comparison to the outer Van Allen radiation belt around Earth. However, in contrast to the Van Allen radiation belt, the duration within the radiation environment on Europa cannot be minimised and the rover has to be designed to withstand the entire mission duration of 30 days.

In order to design and evaluate different radiation protection approaches, different calculations have to be performed. For this purpose the ESA SPace ENVironment Information System (SPENVIS) is used [Platzhalter]. All calculations and figures in Section 4.7 are performed with SPENVIS unless otherwise stated.

4.7.1 Radiation Protection

Various options are available to protect the rover against the radiation. A common approach is the use of aluminium or titanium as these materials can also act as structural elements. However, due to the mass constraints of 30 kg other materials or material compositions are taken in consideration which are more mass effective. In Table 4.7, an optimised shield structure is presented for different weight thresholds designed for the radiation environment around Jupiter. The difference between an aluminium or titanium shielding and an optimised structure listed in Table 4.7 for the total ionizing dose (TID) is shown in Figure F.2.

Due to the mass savings of the optimised structure it will be used where the radiation protection of the aluminium structure is not sufficient. In order to reduce the mass further, a radiation vault is utilised that highly sensible components do not have to be shielded separately.

Table 4.7: Optimal shield structure for an Jupiter mission. [Platzhalter]

| Areal Density / g/cm ² | 0.5 | 1 | 2 | 3 |
|--------------------------------------|-------------|-------------|-------------|-------------|
| Layer No. 1 / mm | Pb 0.415 | Pb 0.829 | W 0.984 | Ta 1.563 |
| Layer No. 2 / mm | Fe 0.033 | Mg 0.158 | Mg 0.540 | Al 0.399 |
| Layer No. 3 / mm | - | - | - | Mg 0.150 |

4.7.2 Components

Every component on the rover has a different radiation tolerance and therefore have to be placed at different compartments within the rover. The radiation tolerances are listed in Table F.1. None sensitive components like the electric motors and harness are only shielded by an aluminium structure where components like the metal within the wire are resistant against the radiation. However, isolators around the cables have to be selected to be resistant in order to prevent short circuits. Highly sensitive components like cameras have an additional protective layer in order to reduce the TID to under 30 krad. Components which are within the rover like the on-board computer (OBC) are placed within the radiation vault which reduces the TID to under 20 krad. For this purpose the optimised shield structure with a weight target of 0.5 g/cm² is used. Detailed TIDs for all components are shown in Figure F.3.

4.7.3 Improvements

Even though the radiation protection is sufficient for the rover to survive at least the nominal mission of 30 days, further improvements can be performed in order to extend the secondary mission.

Local shielding can be applied on less resistant components in order to reduce the wall thickness of the whole radiation wall. If components with a radiation tolerance under 43.27 krad are individually shielded a mass saving of 736.2 g can be achieved. Additionally, water ice extracted from the surface of Europa can be used to improve the radiation protection. With a layer of one centimetre of water, the TID within the radiation vault can be reduced to 16.03 krad without the additional radiation protection beside the 4 mm of aluminium structure. The start mass of the rover can therefore be reduced by 897.2 g by removing the additional shielding.

Detailed calculations for local shielding and water improvements can be found in Appendix F.3 and may be analysed further in Phase B.

4.7.4 Conclusion

In order to protect the rover against the high radiation levels at the surface of Europa, the rover has different compartments. High sensible components are placed within a radiation vault which has a mass optimised structure. Components which have to be outside the radiation vault but are highly sensible are shielded individually. Low sensible Components are protected by the Aluminium structure. Figure 4.9 illustrates the different compartments within the rover and the accorded TIDs.

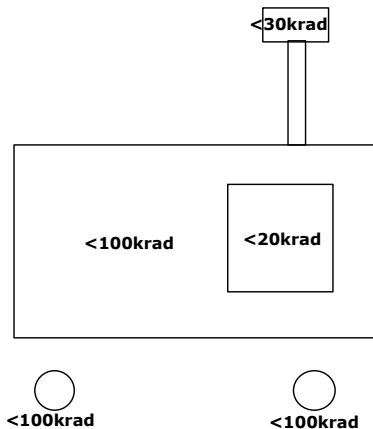


Figure 4.9: Overview of TIDs within different compartments within the rover.

Chapter 5

Outlook & Risk Assessment

5.1 Risk Assessment

To reduce risks and increase the robustness within the development process of the INSPIRE mission, all subsystems focus on flight proven or space grade hard ware. Table 5.1 provides an overview on the TRL of each subsystem.

| Subsystem | overall TRL | Deviating component |
|---------------------|-------------|--|
| Payload | 0 | Drill System and Sample Analyser TRL 0 |
| Structure & Mechan. | 9 | Boom Mechanism TRL 0 |
| Locomotion | 9 | none |
| EPS | 9 | PCDU may be customized |
| TCS | 9 | none |
| COMs, C&DH | 9 | Housekeeping TRL 0 |

Table 5.1: Subsystem TRL for risk assessment

Housekeeping electronics and the Boom Mechanism to extend the camera head for the INSPIRE mission will be custom designed components and therefore rated at TRL 0. However due to proven development processes and simple testing the risk for the mission progress is rated non critical.

Payload components development depict the highest risk for the mission. The Analyser for the ice core samples is a downsized replica of the [missing reference]. The ice core drill derives from the Nano Drill offered by Honeybee Robotics [Missing reference]. Although the technology is available, the drill has to be adapted and tested. Testing in analog conditions could take place in the arctic region and therefore lengthen the mission development process.

As a conclusion the payload subsystem development contains the highest risk for the INSPIRE mission. However the risk is considered manageable. Additionally investing in payload development is regarded worth the risk taking as it is integral to the successful investigation of Europa.

5.2 Outlook

Bibliography

- [1] Jet Propulsion Laboratory. *Galileo Mission to Jupiter*. [online] \url{https://www.jpl.nasa.gov/missions/galileo}.
- [2] NASA Science. *Europa Ocean Moon*. [online] \url{https://solarsystem.nasa.gov/moons/jupiter-moons/europa/in-depth/}.
- [3] Institut für Planetenforschung, DLR. *Die Mission JUICE zum Jupitersystem*. [online] \url{https://www.dlr.de/pf/desktopdefault.aspx/tabid-10617/18438_read-43016/}.
- [4] NASA. *Europa Lander*. [online] \url{https://europa.nasa.gov/}.
- [5] NASA / JPL. *Europa*. [online] \url{https://www.jpl.nasa.gov/missions/europa-lander}.
- [6] Fraunhofer Institute for Solar Energy Systems ISE. *RadHard Project Website*. 2021. [online] \url{https://radhard.org/}.
- [7] R. Abelson et al. *Enabling Exploration with Small Radioisotope Power Systems*. Ed. by NASA JPL. 2004.
- [8] S. Magdum. *Model Based Development of The Enhanced Multi-Mission Radioisotope Thermoelectric Generator and Effect of Thermoelectric Element Length on eMMRTG*. Ed. by Western Michigan University. 2019. [online] \url{http://homepages.wmich.edu/~leehs/ME539/Final%20Presentation%20on%20eMMRTG.pdf}.
- [9] Holgate, T. C.; Bennett, R.; Hammel, T.; Caillat, T.; Keyser, S., and Sievers, B. “Increasing the Efficiency of the Multi-mission Radioisotope Thermoelectric Generator”. In: *Journal of Electronic Materials* 44.6 (2015), pp. 1814–1821. ISSN: 0361-5235. DOI: \url{10.1007/s11664-014-3564-9}.
- [10] JPL NASA. *Enhanced Multi-Mission Radioisotope Thermoelectric Generator (eMMRTG) Concept*. Ed. by NASA JPL. 2014. [online] \url{https://rps.nasa.gov/resources/56/enhanced-multi-mission-radioisotope-thermoelectric-generator-emmrtg-concept/}.
- [11] Lakdawalla, E. *The Design and Engineering of Curiosity*. Cham: Springer International Publishing, 2018. ISBN: 978-3-319-68144-3. DOI: \url{10.1007/978-3-319-68146-7}.
- [12] S. Fasoulas et al. *Lecture Series: Energy Systems for Space Application SS 2020*. 2020.
- [13] S. Klinkner; P. Winterhalder, and M.Nitz et al. *Lecture Series - Rover System Technology SS2021*. 2021.
- [14] SAFT Batteries. *Datasheet - SAFT MP 176065 xlr*. 2018. [online] \url{https://www.saftbatteries.com/products-solutions/products/mp-small-v1}.
- [15] Bradford Space. *Datasheet - Nova PCDU*. Ed. by BRADFORD ENGINEERING BV. 2019. [online] \url{https://satsearch.co/products/bradford-nova-pcdu}.
- [16] “The surface temperature of Europa”. In: *Heliyon* 5.6 (2019), e01908. ISSN: 2405-8440. DOI: \url{https://doi.org/10.1016/j.heliyon.2019.e01908}.
- [17] Thermal Space and Thermal Straps. *Graphene Thermal LyNX® Technology*. [online] \url{https://thermal-space.com/thermal-lynx/}.
- [18] NASA. *Light-Weight Radioisotope Heater Unit*. [online] \url{https://rps.nasa.gov/power-and-thermal-systems/thermal-systems/light-weight-radioisotope-heater-unit/}.

- [19] NASA / JPL. *Aerogel*. [online] \url{https://solarsystem.nasa.gov/stardust/aerogel_factsheet.pdf}.
- [20] Milanze, F. H. and Mantelli, M. B. "Theoretical and experimental studies of a bi-metallic heat switch for space applications ". In: *International Journal of Heat and Mass Transfer* 46.24 (2003), pp. 4573–4586. ISSN: 0017-9310. DOI: [https://doi.org/10.1016/S0017-9310\(03\)00294-1](https://doi.org/10.1016/S0017-9310(03)00294-1).
- [21] S. Klinkner date = 2020, t. T. i. I.
- [22] Aluminium Giesserei Hannover GmbH. *Produktdatenblatt AA5083*. [online] https://www.leichtmetall.eu/site/assets/files/datenblatt/5083_Produktdatenblatt_A4.pdf.
- [23] Aluminium Giesserei Hannover GmbH. *Produktdatenblatt AA6082*. [online] https://www.leichtmetall.eu/site/assets/files/datenblatt/6082_Produktdatenblatt_A4.pdf.
- [24] Aluminium Giesserei Hannover GmbH. *Produktdatenblatt AA7075*. [online] https://www.leichtmetall.eu/site/assets/files/datenblatt/7075_Produktdatenblatt_A4.pdf.
- [25] Deutsche Edelstahlwerke. *1.4418X4 - CrNiMo16-5-1*. [online] \url{https://www.dew-stahl.com/fileadmin/files/dew-stahl.com/documents/Publikationen/Werkstoffdatenblaetter/Luft_Raumfahrt/1.4418_de.pdf}.
- [26] Deutsche Edelstahlwerke. *Firmodur 7225*. [online] \url{https://www.dew-stahl.com/fileadmin/files/dew-stahl.com/documents/Publikationen/Werkstoffdatenblaetter/Baustahl/1.7225_1.7227_de.pdf}.
- [27] thyssenkrupp Material Schweiz. *Titan 6Al4V "ELI"*. [online] \url{https://d2zo35mdb530wx.cloudfront.net/_binary/UCPthyssenkruppBAMXSchweiz/de/downloads/werkstoffdatenblaetter-titan/link-titan_grade_5_elis.pdf}.
- [28] thyssenkrupp Material Schweiz. *Titan Grade 5*. [online] \url{https://d2zo35mdb530wx.cloudfront.net/_binary/UCPthyssenkruppBAMXSchweiz/de/downloads/werkstoffdatenblaetter-titan/link-titan_grade_5.pdf}.

Appendix

A Structure and Mechanism

B Locomotion

B.1 Locomotion Design Drivers

| | mass | low complexity | TRL | energy efficiency | traction | sum | weighting factor [%] | | | | | |
|---------------------|------|----------------|-----|--------------------------|----------|-------|----------------------|--------------------|----------|----------|--------|------|
| criteria | mass | + | + | 0 | 0 | 2 | 28.6% | locomotion systems | 4 wheels | 6 wheels | tracks | legs |
| low complexity | - | + | - | - | - | 1 | 14.3% | | | | | |
| TRL | 0 | - | + | + | - | 1 | 14.3% | | | | | |
| energy efficiency | 0 | + | - | - | 0 | 1 | 14.3% | | | | | |
| traction | 0 | + | + | 0 | 0 | 2 | 28.6% | | | | | |
| Total number of "+" | | 7 | | weighting of one "+" [%] | | 14.3% | | | | | | |
| Legende | | | | | | | | | | | | |
| Pkt. | % | | | | | | | | | | | |
| 2 | >80 | | | | | | | | | | | |
| 1 | >40 | | | | | | | | | | | |
| 0 | <40 | | | | | | | | | | | |

Figure B.1: Trade-off of the locomotion movement system. The criteria with the respective weighting factors are shown on the left. On the right side are the respective systems.

| Terrain | Moisture Content (%) | n | k_c | | k_ϕ | | c | | ϕ | |
|--|----------------------|------|-----------------------|---------------------|-----------------------|---------------------|---------------------|-------|--------|--|
| | | | lb/in. ⁿ⁺¹ | kN/m ⁿ⁺¹ | lb/in. ⁿ⁺² | kN/m ⁿ⁺² | lb/in. ² | kPa | deg | |
| Dry sand (Land Locomotion Lab., LLL) | 0 | 1.1 | 0.1 | 0.99 | 3.9 | 1528.43 | 0.15 | 1.04 | 28° | |
| Sandy loam (LLL) | 15 | 0.7 | 2.3 | 5.27 | 16.8 | 1515.04 | 0.25 | 1.72 | 29° | |
| Sandy loam Michigan (Strong, Buchele) | 22 | 0.2 | 7 | 2.56 | 3 | 43.12 | 0.2 | 1.38 | 38° | |
| Sandy loam (Hanamoto) | 11 | 0.9 | 11 | 52.53 | 6 | 1127.97 | 0.7 | 4.83 | 20° | |
| Clayey soil (Thailand) | 23 | 0.4 | 15 | 11.42 | 27 | 808.96 | 1.4 | 9.65 | 35° | |
| Heavy clay (Waterways Experiment Stn., WES) | 26 | 0.3 | 5.3 | 2.79 | 6.8 | 141.11 | 2.0 | 13.79 | 22° | |
| Lean clay (WES) | 32 | 0.5 | 0.7 | 0.77 | 1.2 | 51.91 | 0.75 | 5.17 | 11° | |
| LETE sand (Wong) | 38 | 0.5 | 12 | 13.19 | 16 | 692.15 | 0.6 | 4.14 | 13° | |
| Upland sandy loam (Wong) | 55 | 0.7 | 7 | 16.03 | 14 | 1262.53 | 0.3 | 2.07 | 10° | |
| Rubicon sandy loam (Wong) | 25 | 0.13 | 45 | 12.70 | 140 | 1555.95 | 10 | 68.95 | 34° | |
| North Gower clayey loam (Wong) | 40 | 0.11 | 7 | 1.84 | 10 | 103.27 | 3 | 20.69 | 6° | |
| Grenville loam (Wong) | 22 | 0.2 | 45 | 16.43 | 120 | 1724.69 | 10 | 68.95 | 20° | |
| Snow (U.S.) (Harrison) | 1.6 | 0.07 | 32 | 102 | 42.2 | 5301 | 0.19 | 1.3 | 31.1° | |
| Snow (Sweden) | 1.6 | 0.04 | 7.5 | 74.6 | 5.3 | 2080 | 0.48 | 3.3 | 33.7° | |
| | 1.44 | 0.3 | 3.5 | 6.9 | 9.7 | 752 | 0.54 | 3.7 | 29.8° | |

Figure B.2: Soil Parameters

Mean Maximum Pressure

Ackerman Steering

Table B.1

| Steering Angle | Mode 1 | Mode 2 | Mode 3 |
|----------------|--------|--------|--------|
| θ_o | | | |
| θ_o | | | |

| Wheel Width [m] | Wheel Diameter [m] | Weight per Wheel [g] |
|-----------------|--------------------|----------------------|
| 0.0500 | 0.1000 | 127 |
| 0.0600 | 0.1000 | 153 |
| 0.0700 | 0.1000 | 178 |
| 0.0800 | 0.1000 | 204 |
| 0.0900 | 0.1000 | 229 |
| 0.1000 | 0.1000 | 265 |
| 0.1500 | 0.1000 | 396 |
| 0.2000 | 0.1000 | 527 |
| 0.2500 | 0.1000 | 658 |
| 0.3000 | 0.1000 | 790 |
| 0.0500 | 0.1250 | 154 |
| 0.0600 | 0.1250 | 185 |
| 0.0700 | 0.1250 | 217 |
| 0.0800 | 0.1250 | 247 |
| 0.0900 | 0.1250 | 278 |
| 0.1000 | 0.1250 | 309 |
| 0.0500 | 0.1500 | 185 |
| 0.0600 | 0.1500 | 221 |
| 0.0700 | 0.1500 | 258 |
| 0.0800 | 0.1500 | 294 |
| 0.0900 | 0.1500 | 331 |
| 0.1000 | 0.1500 | 367 |
| 0.1500 | 0.1500 | 570 |
| 0.2000 | 0.1500 | 760 |
| 0.2500 | 0.1500 | 949 |
| 0.3000 | 0.1500 | 1138 |
| 0.0500 | 0.2000 | 236 |
| 0.0600 | 0.2000 | 284 |
| 0.0700 | 0.2000 | 332 |
| 0.0800 | 0.2000 | 379 |
| 0.0900 | 0.2000 | 427 |
| 0.1000 | 0.2000 | 487 |
| 0.1500 | 0.2000 | 730 |
| 0.2000 | 0.2000 | 973 |
| 0.2500 | 0.2000 | 1215 |
| 0.3000 | 0.2000 | 1458 |

Figure B.3: Various wheel dimensions respective to the weight. Rows highlighted in red are not considered further for system design due to the limit of 200 g weight per wheel.

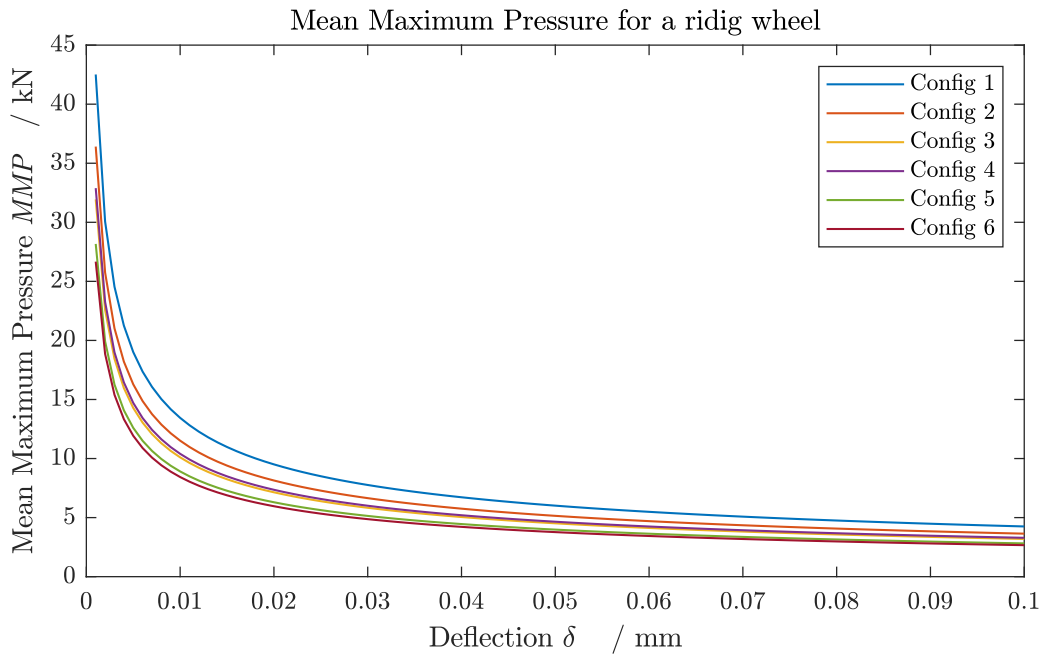


Figure B.4

| Number of axles | Proportion of axles driven | | | | | | |
|-----------------|----------------------------|------|------|------|------|------|------|
| | 1 | 3/4 | 2/3 | 3/5 | ½ | 1/3 | 1/4 |
| 2 | 3.65 | | | | 4.40 | | |
| 3 | 3.90 | | 4.35 | | | 5.25 | |
| 4 | 4.10 | 4.44 | | | 4.95 | | 6.05 |
| 5 | 4.32 | | | 4.97 | | | |
| 6 | 4.6 | | 5.15 | | 5.55 | 6.20 | |

Figure B.5: Parameters for the mean maximum pressure for a wheeled rover.

C Electrical Power System

Table C.1: INSPIRE battery parameters.

| SAFT 176065 xlr [14] | |
|---|---------------|
| Configuration: | |
| Battery Configuration | <i>3s4p</i> |
| Cells in Series s N [-] | 3 |
| Cells in Parallel p M [-] | 4 |
| Cell Parameters: | |
| Typical Cell Capacity [Ah] | 6.8 |
| Nominal Cell Voltage [V] | 3.65 |
| Nominal Cell Capacity [Wh] | 24.8 |
| Typical Cell Mass [kg] | 0.15 |
| Energy Density [Wh/kg] | 165.33 |
| Actual Battery Configuration Parameters: | |
| Battery Voltage V_{Batt} [V] | 10.95 |
| Battery Nominal Capacity E_{Batt} [Wh] | 297.6 |
| Battery Mass [kg] | 1.8 |
| Battery Mass m_{Batt} (incl. 10% Margin) [kg] | 1.98 |
| Configruation according to ECSS reliability restrictions and margins included: | |
| Battery Configuration | <i>3s3p</i> |
| Cells in Series s N [-] | 3 |
| Cells in Parallel p M [-] | 3 |
| Battery Voltage V_{Batt} [V] | 10.95 |
| Battery Nominal Capacity E_{Batt} [Wh] | 231.60 |
| 30% Margin on Energy Content | 0.3 |
| Battery Nominal Capacity E_{Batt} incl. Margin [Wh] | 156.24 |
| Useable Energy Density [Wh/kg] | 78.91 |

Figure C.1: Holistic Power Budget of INPSIRE.

D Communications

D.1 Link Budget

Link budget considerations are performed under the conservative assumptions listed in Table D.1.

| Parameter | Value | Unit | Symbol | Source |
|---------------------------------|--------|-----------|----------|------------------------------|
| Rover | | | | |
| antenna Gain | 2 | [dB] | G_R | omnidirectional LGA |
| output power | 1 | [W] | P_R | |
| line loss | 0,6 | [dB] | L_{l1} | FLP |
| Path | | | | |
| R2L polarisation loss | 0,3 | [dB] | L_p | FLP |
| free space loss | 117,55 | [m^3] | L_s | |
| atmospheric loss | 0 | [dB] | L_a | negligible atmosphere |
| Lander | | | | |
| antenna Gain | 1 | [dB] | G_L | conservative estimation |
| output power | 5 | [W] | P_L | conservative estimation |
| pointing Loss | 0 | [dB] | n/a | omnidirectional LGA |
| line Loss | 0,6 | [dB] | L_{l2} | FLP |
| eff. noise temperature | 300 | [K] | T_s | worst case E-bay temperature |
| Demodulation & Uncertain Losses | | | | |
| eff. data rate | 5000 | [kbps] | R | |
| FEC coding | none | [-] | n/a | |
| technical degradation | 1 | [dB] | L_{i1} | FLP |
| implementation loss | 1 | [dB] | L_{i1} | FLP |

Table D.1: Transmission link parameters

The free space loss L_s [m^3] in Table D.1 is calculated using the following correlation.

$$L_s = \frac{(4\pi s)^2 \cdot c}{f} \quad (5.1)$$

The signal travel distance s is assumed to be $s = 2000 \text{ m}$ which is in excess of the mission goal. In accordance with X-Band communication the frequency f is set to a value of $f = 8,2 \text{ GHz}$. The parameter c represents the speed of light in vacuum. For simplification purposes $c = 3 \cdot 10^9 \frac{\text{m}}{\text{s}}$ is assumed.

Combining the parameters from Table D.1 the link budget is calculated using Equation 5.2. For the simplification of Equation 5.2 the line losses for the rover L_{l1} and lander L_{l2} are expressed as the sum L_l . In the same manner technical degradation and implementation losses are combined to L_i . Atmospheric losses L_a and pointing errors in Equation 5.2 are neglected due to a lack of atmosphere and the utilisation of omnidirectional low gain antennas. Parameter k describes the Boltzmann constant.

$$\frac{E_b}{N_0} = P - L_l + G_R - 10 \cdot \log L_s - L_a + G_L + 10 \cdot \log k - 10 \cdot \log T_s - 10 \cdot \log R - L_i \quad (5.2)$$

Equation 5.2 and the conservative assumptions from Table D.1 results in an energy per bit over noise $\frac{E_b}{N_0} = 10,59 \text{ dB}$. The complete link budget can be found in Figure D.1.

Referencing Figure D.3 a Bit Error Rate of 10^{-4} can be achieved in the downlink path, which is considered sufficient for a first assessment. Optionally a FEC code can be implemented in later design phases.

Using the same parameters listed in Table D.1 leads to a $\frac{E_b}{N_0} = 50,56 \text{ dB}$ corresponding to a Bit Error Rate of potentially less than 10^{-6} . Therefore the downlink does not contribute to the design decisions. The complete link budget for the uplink path can be found in Figure D.2.

D.2 Mission Data Output

The analysis of the mission data concept for memory capacity and transmission times is focuses on the payload camera and Hazcams as images require far more data than telemetry or other payload data.

In a first assumption 420 images per day are stored and transmitted. Considering the sensor resolution of 2048×2048 pixels and a bit depth per pixel of 10 bit leads to a file size of 42 Mbit per image.

To calculate the message size in Table D.2, it is assumed that a transmission frame consists of 10264 bits including a payload frame of maximum 8840 bits.

| File Type | Compression | File Size | Message Size | Data Rate | Tx t per File |
|-----------|-------------|------------|--------------|-----------|---------------|
| image | none | 42 Mbit | 48,77 Mbit | 5 Mbit | 8,12 s |
| image | HIREW | 23,52 Mbit | 27,31 Mbit | 5 Mbit | 5,45 s |

Table D.2: Comparison of transmission times per image (message frame bits included)

| File per tal | Compression | File Size | Total Data | Tx time |
|--------------|-------------|------------|------------|------------|
| 420 | none | 42 Mbit | 2,21 GB | 56,9 Min. |
| 420 | HIREW | 23,52 Mbit | 1,22 GB | 38,23 Min. |

Table D.3: Transmission time and total data output per tal

The HIREW compression algorithm is suggested for the mission considering a high average compression of 0,56 % and a high compression speed of 123 Mbit/s for grayscale and 104,4 Mbit/s for RGB image files.

D.3 Communications Trade Off

Transmitter Selection

Receiver Trade Off

Antenna Trade Off

D.4 Command & Data Handling Trade Off

OBC Trade Off

| | | |
|---|------|--------------|
| Rover Transmitter Output Power | | 1 Watts |
| | | 0,00 dBW |
| Rover total Line loss | | -0,6 dB |
| Rover Antenna Gain | Gr | 2 dBi |
| Rover EIRP | | 1,40 dBW |
| Downlink Path | | |
| Rover antenna pointing loss | | 0 dB |
| R2L polarization loss | | -0,3 dB |
| free space loss | | -116,74 dB |
| atmospheric loss | | 0 dB |
| Signal Level at Lander | RIP | -115,64 dB |
| Lander | | |
| Lander LGA pointing loss | | 0 dB |
| Lander antenna Gain | Gl | 1 dBic |
| Signal after Lander LGA | | -114,64 dB |
| Lander total line loss | | -0,6 dB |
| Lander effective noise temperature | | -24,77 dB |
| Lander signal to noise power density | C/No | 88,58 dB |
| Data Rate | | |
| data rate | | 5000 kbps |
| | | -66,99 dBHz |
| Total | | |
| System Eb/N0 for Rover to Lander link | | 21,59 dB |
| Demodulation | | |
| specified Bit Error Rate | | 1,00E-04 n/a |
| FEC coding | | none |
| Eb/N0 threshold | | 9 dB |
| Uncertain Losses | | |
| technical degradation of equipment | | 1 dB |
| implementation loss | | 1 dB |
| Total | | |
| system Link Margin after uncertain losses | | 10,59 dB |

Figure D.1: Rover to Lander complete downlink budget.

| Lander to Rover (L2R) Budget (Lander LGA Antenna) | | |
|---|------|--------------|
| Lander | | |
| Lander Transmitter Output Power | | 5 Watts |
| | | 6,99 dB |
| Lander total Line loss | | -0,6 dB |
| Lander Antenna Gain | G_L | 1 dBi |
| Lander EIRP | | 7,39 dBW |
| Uplink Path | | |
| Lander Antenna Pointing loss | | 0 dB |
| L2R polarization loss | | -0,3 dB |
| path loss | | -116,74 dB |
| atmospheric loss | | 0 dB |
| Signal Level at Lander | RIP | -109,65 dB |
| Rover | | |
| Rover LGA pointing loss | | 0 dB |
| Rover Antenna Gain | G_R | 1 dBic |
| Signal after Rover LGA | | -108,65 dB |
| Rover total line loss | | -0,6 dB |
| Rover effective noise temperature | | -24,77 dB |
| Rover signal to noise power density | C/No | 94,57 dB |
| data rate | | |
| data rate | | 2 kbps |
| | | -33,01 dBHz |
| Total | | |
| System Eb/N0 for Lander to Rover link | | 61,56 dB |
| demodulation | | |
| Specified Bit Error Rate | | 1,00E-04 n/a |
| FEC coding used | | none |
| Eb/N0 threshold | | 9 dB |
| uncertain losses | | |
| Technical degradation of equipment | | 1 dB |
| Implementation loss | | 1 dB |
| Total | | |
| System Link Margin after uncertain losses | | 50,56 dB |

Figure D.2: Lander to Rover complete uplink budget.

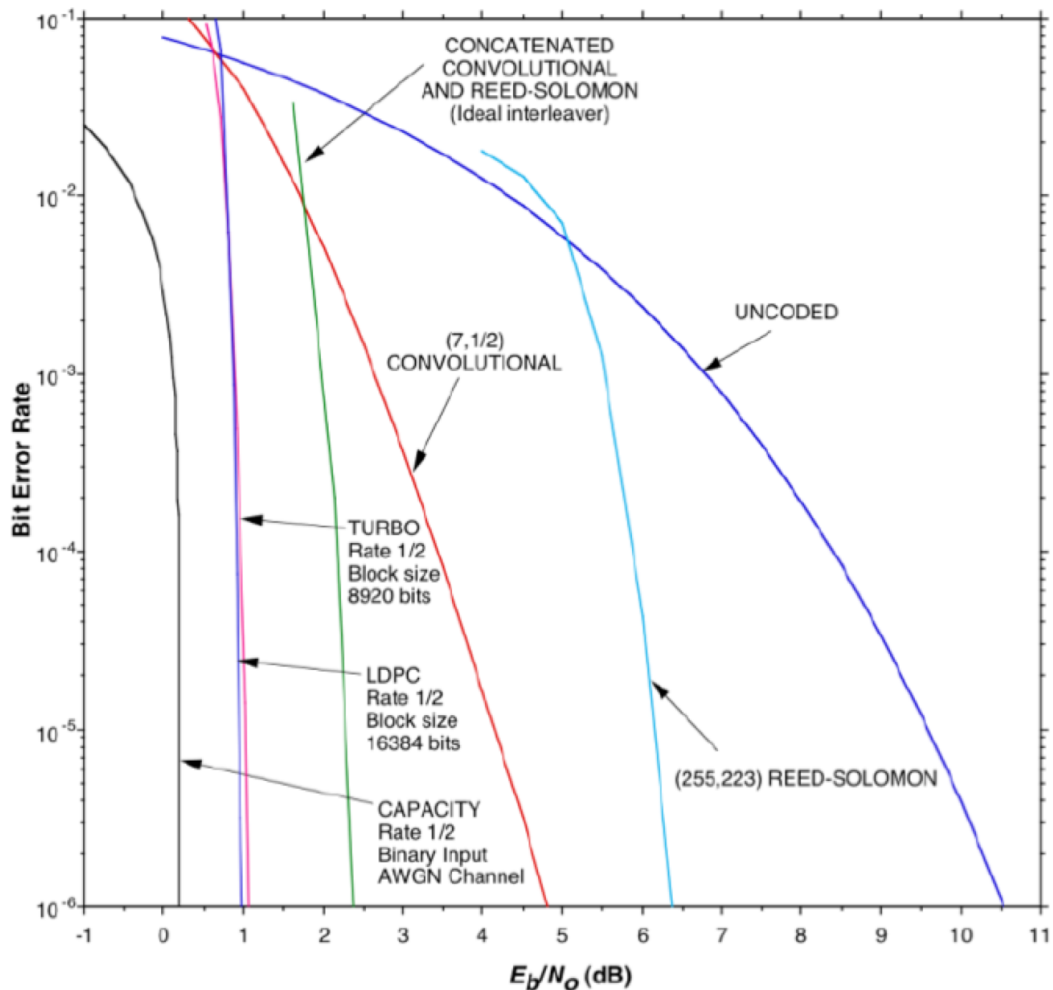


Figure D.3: Bit Error Rate for different FEC codes

D. COMMUNICATIONS

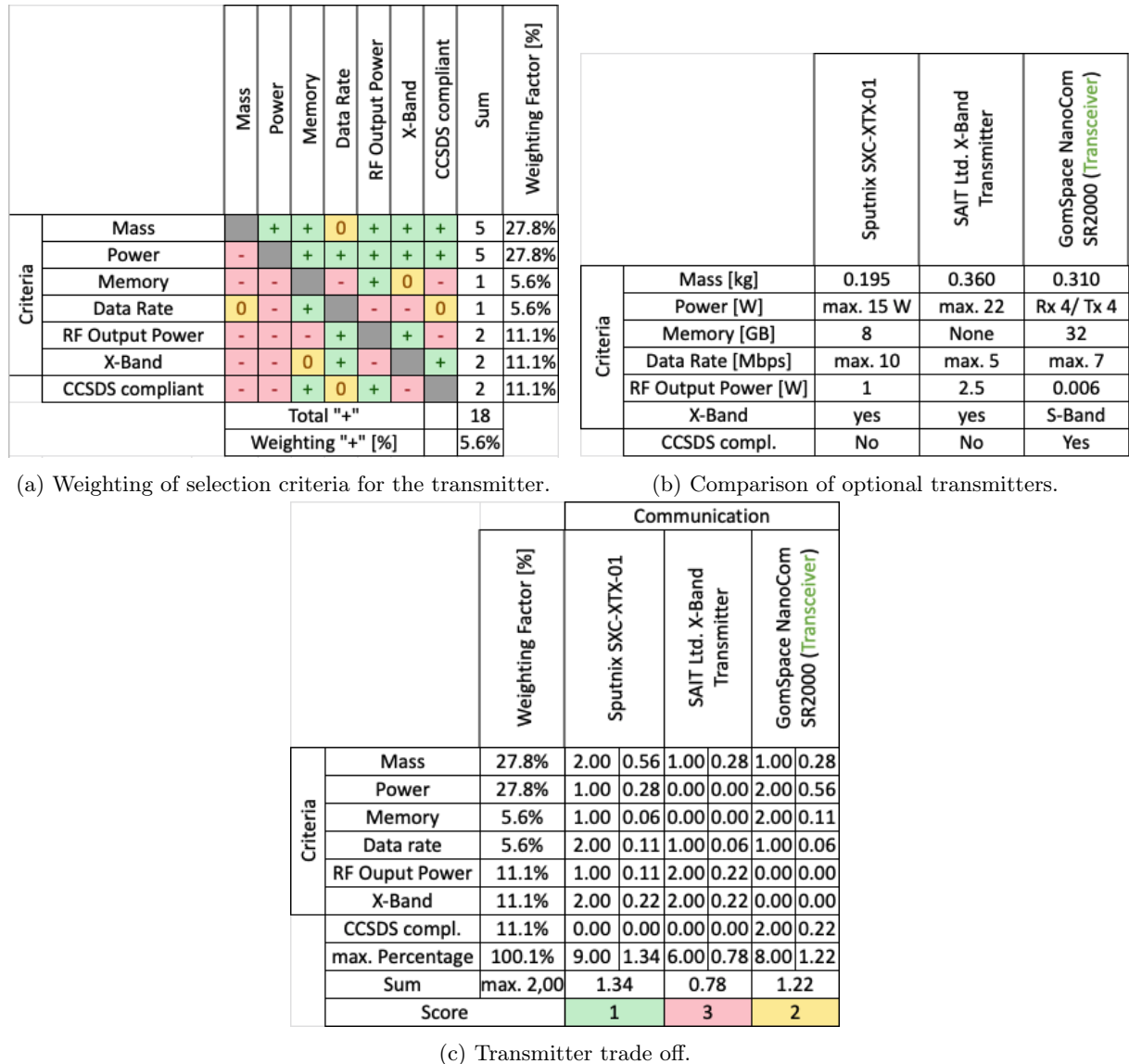


Figure D.4: Transmitter Trade off for the Communication subsystem.

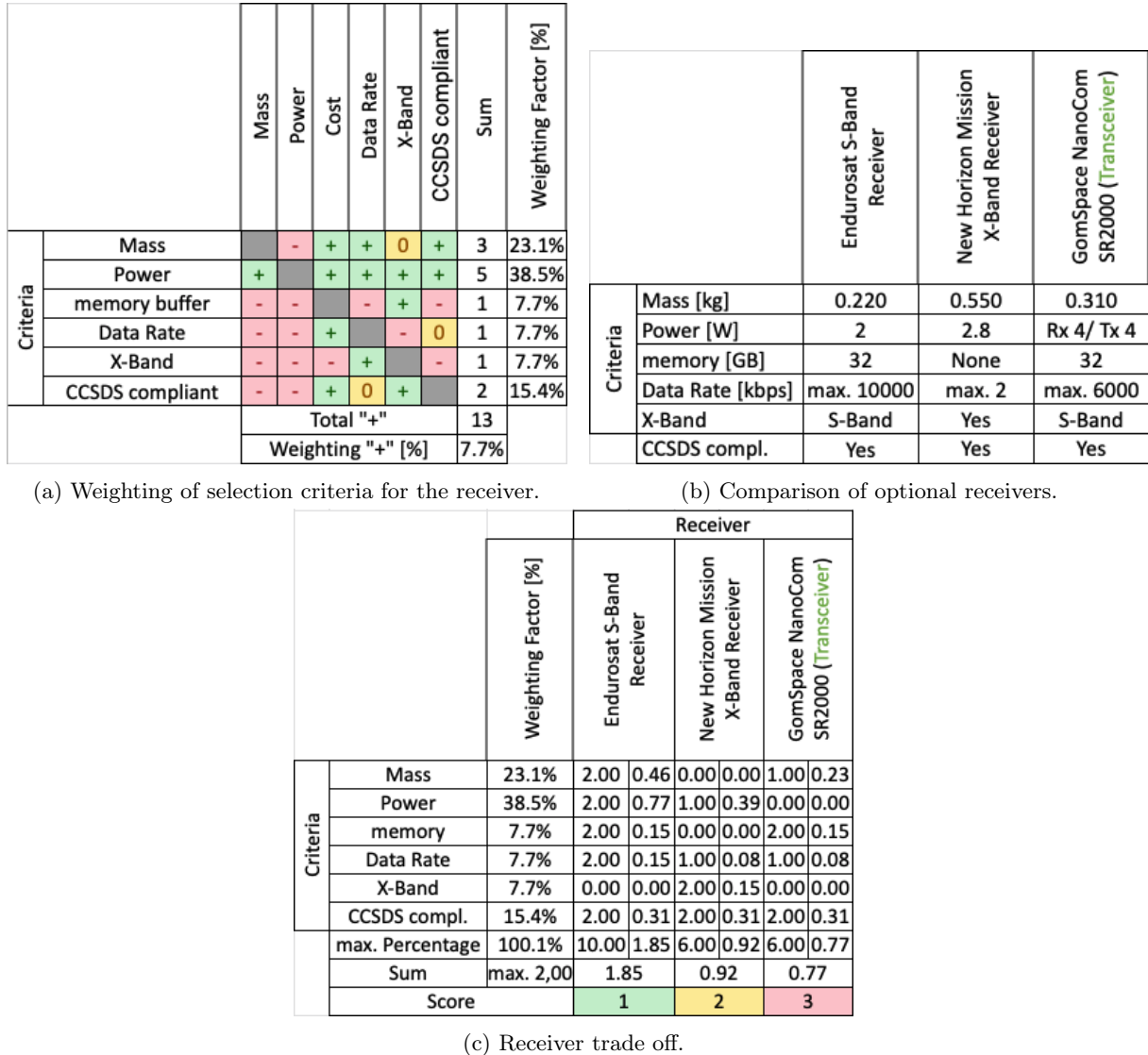


Figure D.5: Receiver Trade off for the Communication subsystem.

D. COMMUNICATIONS

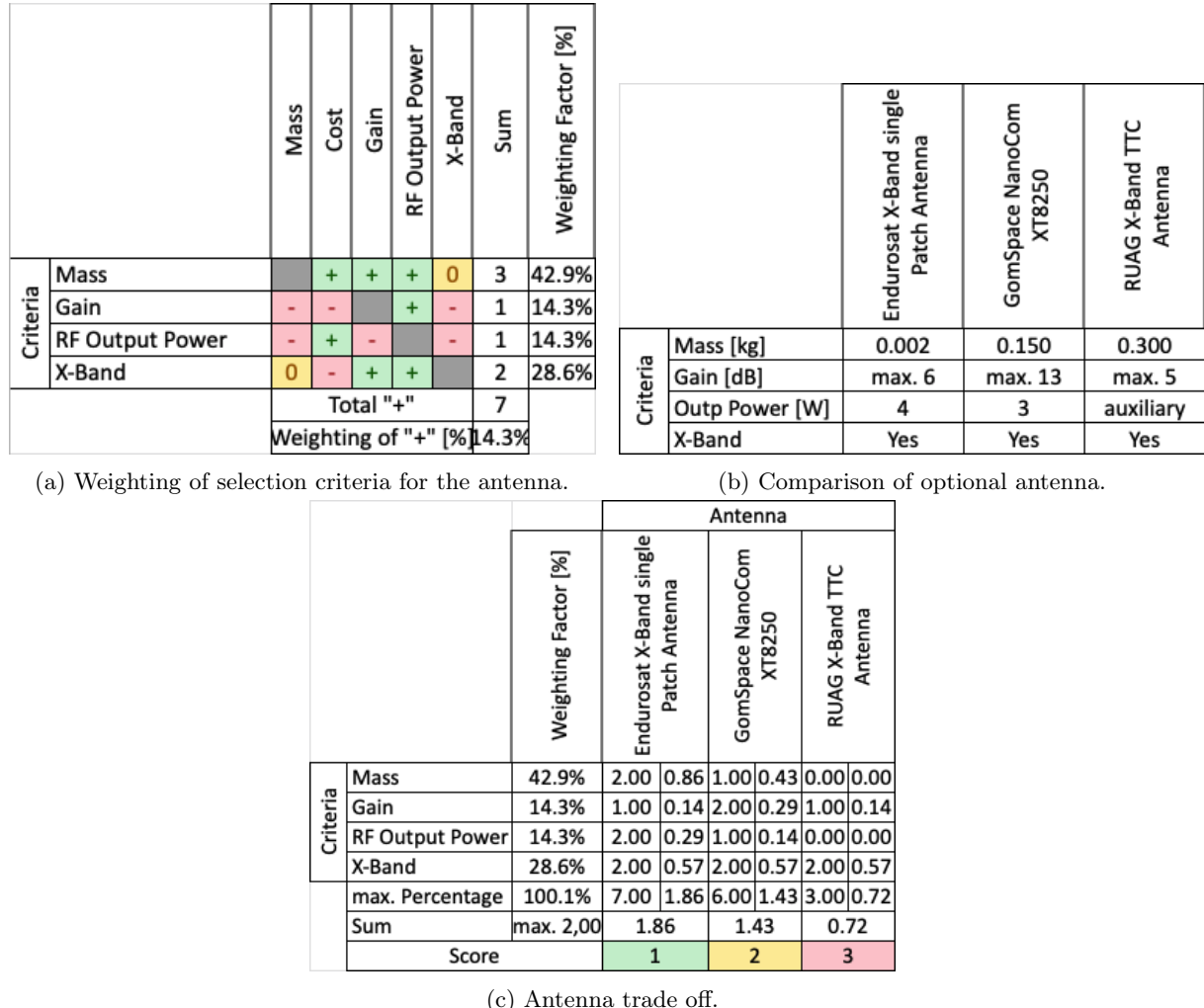


Figure D.6: Antenna trade off for the Communication subsystem.

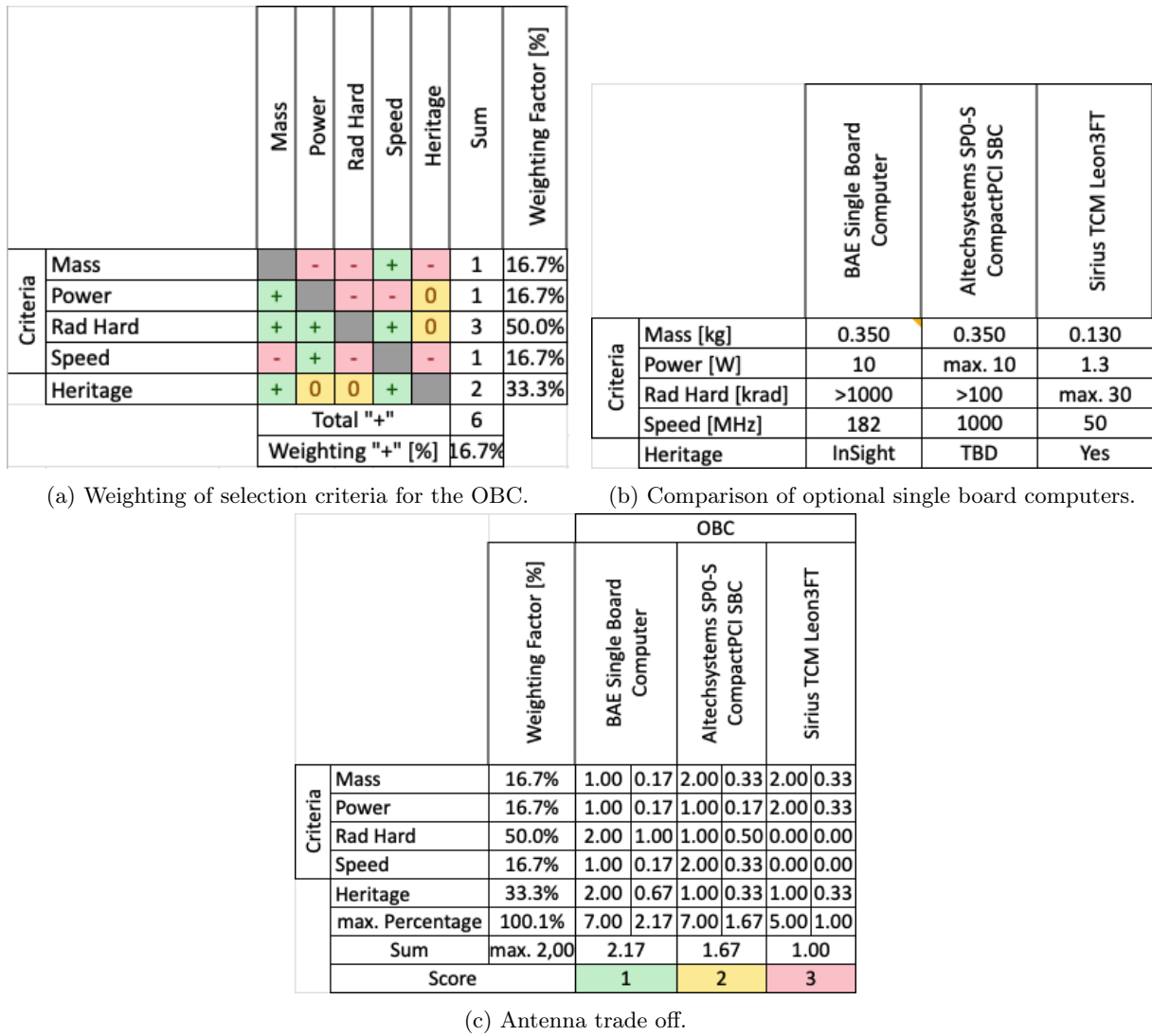


Figure D.7: OBC trade off for the Command & Data Handling subsystem.

E Thermal Controls System

E.1 Heat energy eqilibrium

The follwing equiations describe each node of the thermal network. The input values were tanken from EPS, Subsection E.2, Subsection E.3, Subsection E.4 respectively.

RTG:

$$0 = \dot{Q}_{RTG} + CON_1 \cdot (T_{Bay} - T_{RTG}) + CON_2 \cdot (T_{Ch} - T_{RTG}) + \\ + CON_5 \cdot (T_{Drill} - T_{RTG}) - \epsilon_{RTG} \cdot \sigma_b \cdot S_{RTG} \cdot T_{RTG}^4 \quad (5.3)$$

Electric Bay: Subscript *Bay*

$$0 = \dot{Q}_{Bay} + CON_1 \cdot (T_{RTG} - T_{Bay}) + CON_3 \cdot (T_{Ch} - T_{Bay}) - \epsilon_{Bay} \cdot \sigma_b \cdot S_{Bay} \cdot T_{Bay}^4 \quad (5.4)$$

with:

$$\dot{Q}_{B,intern} = \dot{Q}_{OBC} + \dot{Q}_{Tranceiver} + \dot{Q}_{Receiver} + \dot{Q}_{PCDU} \quad (5.5)$$

Drill & Analyser:

$$0 = \dot{Q}_{Drill} + CON_4 \cdot (T_{Ch} - T_{Drill}) + CON_5 \cdot (T_{RTG} - T_{Drill}) \quad (5.6)$$

Camera:

$$0 = \dot{Q}_{Cam} + \dot{Q}_{RHU} + CON_6 \cdot (T_{Ch} - T_{Cam}) + \\ + (CON_{14} + n_{S1} \cdot CON_{S1}) \cdot (T_{Rad} - T_{Cam}) - \epsilon_{Cam} \cdot \sigma_b \cdot S_{Cam} \cdot T_{Cam}^4 \quad (5.7)$$

Radiator:

$$(CON_{14} + n_{S1} \cdot CON_{S1}) \cdot (T_{Cam} - T_{Rad}) - \epsilon_{Rad} \cdot \sigma_b \cdot S_{Rad} \cdot T_{Rad}^4 = 0 \quad (5.8)$$

Chassis:

$$0 = \dot{Q}_{Radar} + \dot{Q}_{Hazcam} + CON_2 \cdot (T_{RTG} - T_{Ch}) + CON_3 \cdot (T_{Bay} - T_{Ch}) + \\ + CON_4 \cdot (T_{Drill} - T_{Ch}) + CON_6 \cdot (T_{Cam} - T_{Ch}) + CON_7 \cdot (T_{Node_1} - T_{Ch}) + \\ + \alpha_{Ch} \cdot [S_0 \cdot (1 + \rho_E) \cdot (S_{Ch1} \cdot \varphi_1 + S_{Ch2} \cdot \varphi_2) + \epsilon_E \cdot \sigma_b \cdot S_{Ch3} \cdot T_{Surface}^4] - \\ - \epsilon_{Ch} \cdot \sigma_b \cdot S_{Ch} \cdot T_{Ch}^4 \quad (5.9)$$

Steer Engine:

$$0 = 4 \cdot [\dot{Q}_{E,S} + (CON_8 + n_{S2} \cdot CON_{S2}) \cdot (T_{Node_1} - T_{E,S}) + \\ + CON_9 \cdot (T_{RTG} - T_{E,S}) - \epsilon_{E,S} \cdot \sigma_b \cdot S_{E,S} \cdot T_{E,S}^4] \quad (5.10)$$

Distribution Node 1:

$$0 = 4 \cdot [CON_7 \cdot (T_{Ch} - T_{Node_1}) + CON_8 \cdot (T_{E,S} - T_{Node_1}) + CON_{10} \cdot (T_{Node_2} - T_{Node_1})] \quad (5.11)$$

Drive Engine:

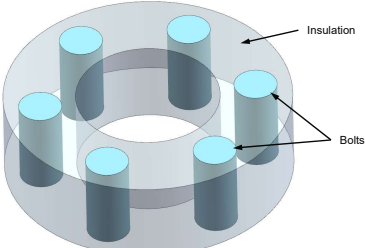
$$0 = 4 \cdot [\dot{Q}_{E,D} + (CON_{11} + n_{S3} \cdot CON_{S3}) \cdot (T_{Node_2} - T_{E,D}) + CON_{12} \cdot (T_{RTG} - T_{E,D}) - \epsilon_{E,D} \cdot \sigma_b \cdot S_{E,D} \cdot T_{E,D}^4] \quad (5.12)$$

Distribution Node 2:

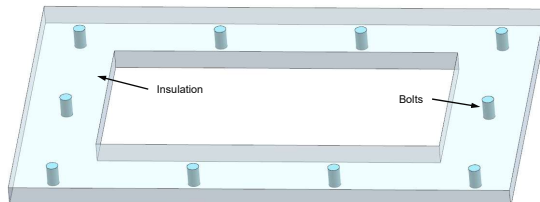
$$0 = 4 \cdot [CON_{10} \cdot (T_{Node_1} - T_{Node_2}) + CON_{11} \cdot (T_{E,D} - T_{Node_2}) + CON_{13} \cdot (T_{Ground} - T_{Node_2})] \quad (5.13)$$

E.2 Heat conductance

Table E.1: Definition of heat conductance C between the nodes according to Figure 4.8.

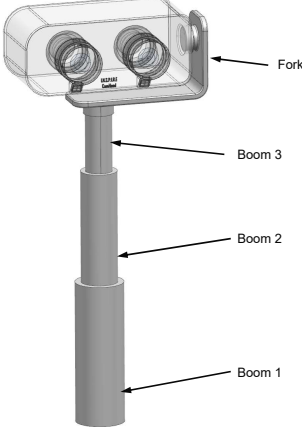
| Name | Linked Components | Geometry |
|----------------|----------------------|--|
| Linkage | RTG ↔ Chassis |  |

| Part | Cross section | Thickness | Material | Amount |
|------------|----------------------------|-----------------------|----------|--------|
| Insulation | $S_I = 3'770 \text{ mm}^2$ | $t_I = 12 \text{ mm}$ | Aerogel | 1 |
| Bolts, M6 | $S_B = 28.3 \text{ mm}^2$ | $t_B = 12 \text{ mm}$ | Titan | 10 |

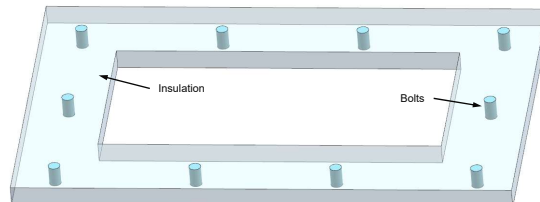
| Name | Linked Components | Geometry |
|----------------|-----------------------|--|
| Linkage | EBay ↔ Chassis |  |

| Part | Cross section | Thickness | Material | Amount |
|------------|-----------------------------|-----------------------|----------|--------|
| Insulation | $S_I = 27'120 \text{ mm}^2$ | $t_I = 12 \text{ mm}$ | Aerogel | 1 |
| Bolts, M6 | $S_B = 28.3 \text{ mm}^2$ | $t_B = 12 \text{ mm}$ | Titan | 10 |

Table E.2: Definition of heat conductance $CON = \frac{1}{R}$ between the nodes according to Figure 4.8.

| Name | Linked Components | Geometry |
|------------------|--|--|
| Telescope | Camera \leftrightarrow Chassis |  <p>$CON_6 = \left(\frac{1}{CON_{B1}} + \frac{1}{CON_{B2}} + \frac{1}{CON_{B3}} + \frac{1}{CON_F} \right)^{-1}$</p> <p>$CON_6 = 7.10 \cdot 10^{-2} \frac{W}{K}$</p> |

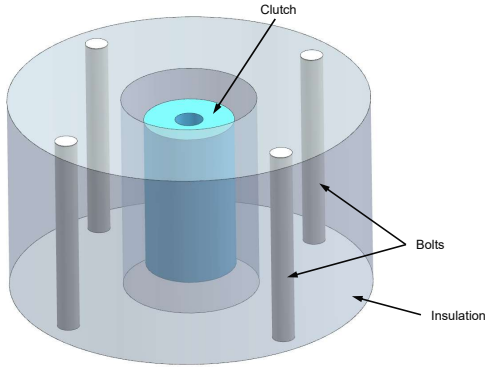
| Part | Cross section | Thickness | Material | Amount |
|--------|-----------------------------|---------------------------|-----------|--------|
| Boom 1 | $S_{B1} = 181 \text{ mm}^2$ | $t_{B1} = 116 \text{ mm}$ | Aluminium | 1 |
| Boom 2 | $S_{B2} = 134 \text{ mm}^2$ | $t_{B2} = 95 \text{ mm}$ | Aluminium | 1 |
| Boom 3 | $S_{B3} = 97 \text{ mm}^2$ | $t_{B3} = 60 \text{ mm}$ | Aluminium | 1 |
| Fork | $S_F = 200 \text{ mm}^2$ | $t_F = 170 \text{ mm}$ | Aluminium | 1 |

| Name | Linked Components | Geometry |
|-------------------|--|---|
| Suspension | Node₁ \leftrightarrow Chassis |  <p>$CON_7 = 1.61 \cdot 10^{-1} \frac{W}{K}$</p> |

| Part | Cross section | Thickness | Material | Amount |
|------------|--------------------------|------------------------|-----------|--------|
| Suspension | $S_S = 137 \text{ mm}^2$ | $t_S = 201 \text{ mm}$ | Aluminium | 1 |

E. THERMAL CONTROLS SYSTEM

Table E.3: Definition of heat conductance $CON = \frac{1}{R}$ between the nodes according to Figure 4.8.

| Name | Linked Components | Geometry | | |
|--|---|-----------------------|-----------|--------|
| Mounting | Steer Engine \leftrightarrow Node₁ | | | |
| $CON_8 = CON_C + CON_I + n_B \cdot CON_B$ | | | | |
| $CON_8 = 6.85 \cdot 10^{-1} \frac{\text{W}}{\text{K}}$ | | | | |
|  | | | | |
| Part | Cross section | Thickness | Material | Amount |
| Clutch | $S_C = 45.4 \text{ mm}^2$ | $t_C = 14 \text{ mm}$ | Aluminium | 1 |
| Insulation | $S_I = 691 \text{ mm}^2$ | $t_I = 18 \text{ mm}$ | Aerogel | 1 |
| Bolts | $S_B = 3.14 \text{ mm}^2$ | $t_B = 18 \text{ mm}$ | Steel | 4 |

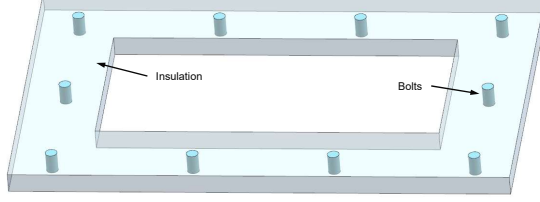
| Name | Linked Components | Geometry | | |
|--|---|----------------|-----------|--------|
| Wheel Fork | Node₁ \leftrightarrow Node₂ | | | |
| $CON_{10} = 2.29 \cdot 10^{-1} \frac{\text{W}}{\text{K}}$ | | | | |
|  | | | | |
| Part | Cross section | Thickness | Material | Amount |
| Wheel Fork | $S_{WF} = 200 \text{ mm}^2$ | $t_{WF} = 175$ | Aluminium | 1 |

Table E.4: Definition of heat conductance $CON = \frac{1}{R}$ between the nodes according to Figure 4.8.

| Name | Linked Components | Geometry |
|-----------------|---|----------|
| Mounting | Drive Engine \leftrightarrow Node₂ $CON_{11} = \left(\frac{1}{CON_G} + \frac{1}{CON_S + CON_I + n_B \cdot CON_B} \right)^{-1}$ $CON_{11} = 2.19 \cdot 10^{-1} \frac{\text{W}}{\text{K}}$ | |

| Part | Cross section | Thickness | Material | Amount |
|------------|---------------------------|-------------------------|----------|--------|
| Gear Box | $S_G = 566 \text{ mm}^2$ | $t_G = 43.1 \text{ mm}$ | Steel | 1 |
| Shaft | $S_S = 23.8 \text{ mm}^2$ | $t_S = 8 \text{ mm}$ | Steel | 1 |
| Insulation | $S_I = 490 \text{ mm}^2$ | $t_I = 8 \text{ mm}$ | Aerogel | 1 |
| Bolts, M3 | $S_B = 7.07 \text{ mm}^2$ | $t_B = 8 \text{ mm}$ | Steel | 4 |

| Name | Linked Components | Geometry |
|------------|--|----------|
| Rim | Node₂ \leftrightarrow Ground $CON_{13} = 5.11 \cdot 10^{-3} \frac{\text{W}}{\text{K}}$ | |

| Part | Cross section | Thickness | Material | Amount |
|------|-------------------------|------------------------|----------|--------|
| Rim | $S_R = 12 \text{ mm}^2$ | $t_r = 100 \text{ mm}$ | Titan | 6 |

Note: It was assumed, that the wheel temperature equals the surface temperature because of the remarkable difference of the heat conduction, $\frac{\lambda_{Wheel}}{\lambda_{Rim}} = 28.2$.

E.3 Heat switch

The characteristic of the switch conductance depends on the mean temperature T_M , shown by measurements in cite . As this temperature won't be calculated in the analysis, the corresponding component temperature T_C shall be used. In order to describe the characteristic, it was divided in three sections, Figure E.1. The temperature where the disk decouples is $T_{toggle} = 108K$ and not applicable for the current application. By reducing the height, the toggle temperature can be increased and the characteristic can be shifted to higher temperatures ("to the right"). It was assumed, that the gradients of section 2 and 3 as well as the temperature range of section 2 keep constant. The axis intersection is a function of the toggle temperature ($a_2 = f(\Delta T_{toggle})$, $\Delta T_{Toggle} = T_{new} - T_{old}|_{toggle}$). The used toggle temperature are listed in autoref

Table E.5: Sections and range of the switch characteristic.

| Section | Temperature range | Heat conductance $CON_S = \frac{1}{R_t}$ |
|---------|-----------------------------|---|
| 1 | $T_{toggle} > T_C$ | $CON_S = 16.4 \cdot 10^{-3} \frac{\text{W}}{\text{m}^2\text{K}} = const.$ |
| 2 | $T_{toggle} \leq T_C < T_1$ | $CON_S(T_C) = a_{1.1} \cdot T_C + a_{1.2}$ $a_{1.1} = +1.272 \cdot 10^{-3} \frac{\text{W}}{\text{m}^2\text{K}^2}$ $a_{1.2} = -1.272 \cdot 10^{-3} \frac{\text{W}}{\text{m}^2\text{K}^2} \cdot \Delta T_{Toggle} - 0.117 \frac{\text{W}}{\text{m}^2\text{K}}$ |
| 3 | $T_C > T_1$ | $CON_S(T_C) = a_{2.1} \cdot T_C + a_{2.2}$ $a_{2.1} = +333 \cdot 10^{-6} \frac{\text{W}}{\text{m}^2\text{K}^2}$ $a_{2.2} = -333 \cdot 10^{-6} \frac{\text{W}}{\text{m}^2\text{K}^2} \cdot \Delta T_{Toggle} - 28.3 \cdot 10^{-3} \frac{\text{W}}{\text{m}^2\text{K}}$ |

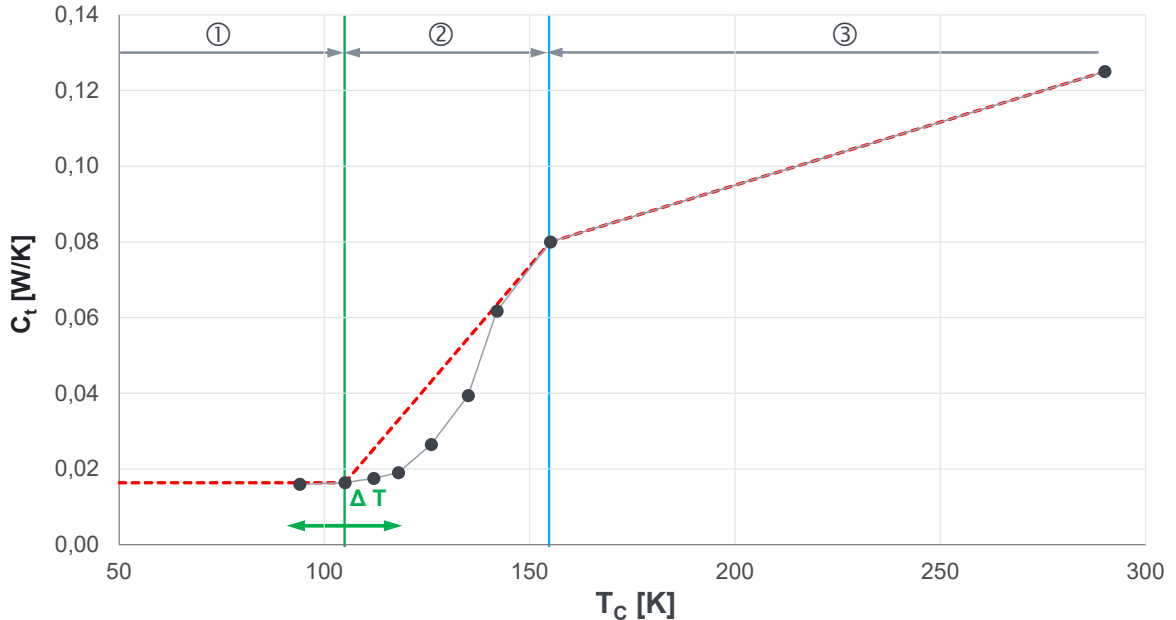


Figure E.1: Conductance characteristic of heat switch divided in sections.

Table E.6: Toggle temperature and amount of bi-metallic heat switch.

| Heat switch name | Linked Components | Temperature | Amount |
|------------------|--|-------------|----------------|
| CON_{S1} | Camera \leftrightarrow Radiator | -20 °C | $n_{S1} = ?1?$ |
| CON_{S2} | Steer Engine \leftrightarrow Node ₁ | -30 °C | $n_{S2} = ?1?$ |
| CON_{S3} | Drive Engine \leftrightarrow Node ₂ | -20 °C | $n_{S3} = ?1?$ |

E.4 Rover absorptivity

The rover position relativ to the direct sun radiation is given by the ecliptic longitude λ_R and latitude δ_R angle, where the axis x_E points always to the sun, Figure E.2b. The amount of solar radiation S_0 absorbed by the rover surfaces depends on the sun altitude and can be determined by the view factor φ , see Figure E.2a. The view factors during eclipse are set to zero.

$$\begin{aligned} \text{View Factor 1, horizontal surface: } & \varphi_1 = \cos(\lambda_R) \cdot \cos(\delta_R) \\ \text{View Factor 2, vertical surface: } & \varphi_2 = \cos(90^\circ - \lambda_R) \cdot \cos(\delta_R) \end{aligned}$$

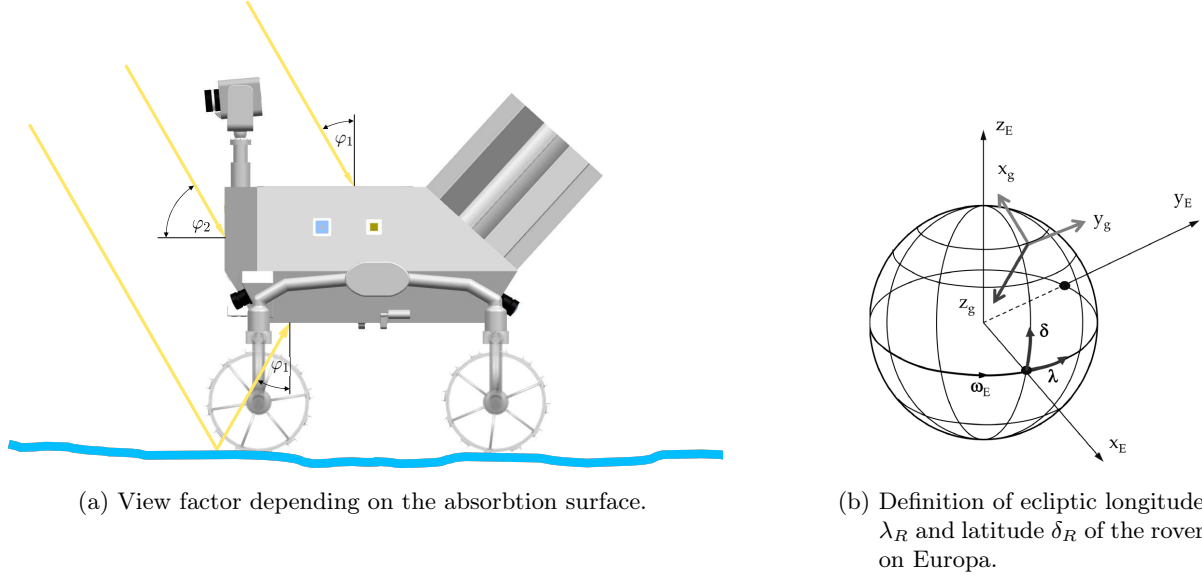


Figure E.2: Bi-metallic heat switch, [20].

E.5 Input Values

The Europa surface temperature varies at the equator between $T_{e,min} = 80$ K and $T_{e,max} = 130$ K, depending on the sun inclination. The temperature at the pole is $T_{Pole} = 50$ K, [16]. It was assumed, that the surface temperature depends on the sun altitude. A trigonometrical interpolation was defined as follows.

$$T_{Surface}(\lambda, \delta) = T_{Pole} + \cos(\delta) \cdot [(T_{e,min} + \cos(\lambda) \cdot (T_{e,max} - T_{e,min})) - T_{Pole}]$$

For λ and δ see Subsection E.4.

Table E.7: Temperatur limits of the rover components.

| Component | Temperature limits in [°C] | | Source |
|-----------------|----------------------------|------|--------|
| | min. | max. | |
| OBC | -55 | 70 | |
| Transmitter | -10 | 50 | |
| Receiver | -30 | 70 | |
| PCDU | -40 | 60 | |
| Battery | -20 | 60 | [14] |
| Camera | -40 | 70 | |
| Objektive | -40 | 71 | |
| Steering Engine | -30 | 100 | |
| Drive Engine | -40 | 100 | |
| Drive Gear | -40 | 100 | |

Table E.8: Minimum and maximum of surface emisivity and absorptivity values, [21].

| Surface finishing | Emisivity [-] | | Absorptivity [-] | |
|-------------------------|---------------|------|------------------|------|
| | min. | max. | min. | max. |
| Aluminium, polished | | 0.05 | | 0.2 |
| Aluminium, sand blasted | | 0.2 | | 0.4 |
| White paint | 0.8 | 0.9 | 0.2 | 0.5 |

Table E.9: Heat conductivity in $\frac{\text{W}}{\text{mK}}$

| Material | Nominal | Used | Source |
|-------------------------|--------------|------|------------------|
| Aerogel | 0.002 - 0.05 | 0.05 | [19] |
| Aluminium ¹⁾ | 110 - 220 | 220 | [22], [23], [24] |
| Steel ¹⁾ | 15 - 43 | 45 | [25], [26] |
| Titan | 7.1 | 7.1 | [27], [28] |

¹⁾ Depends on the alloying component, a conservative value was choosen.

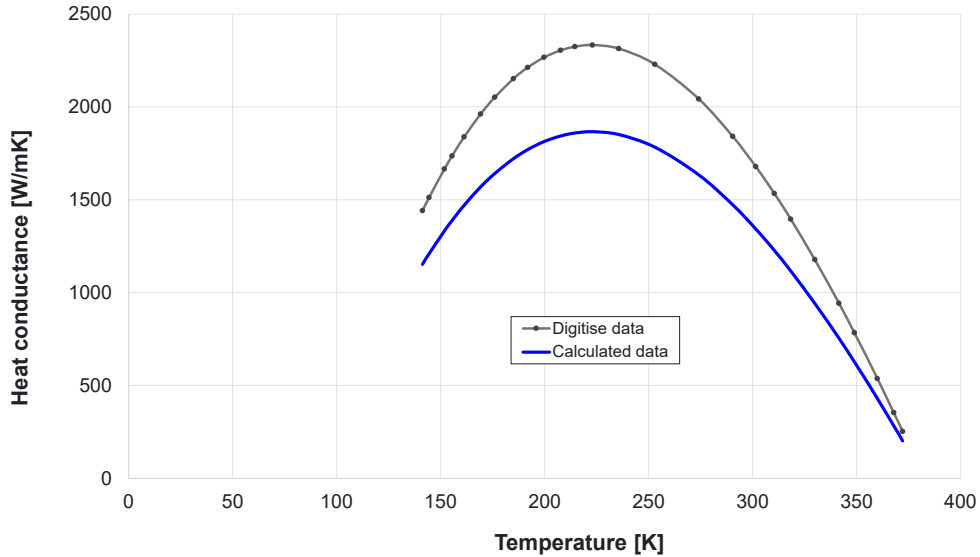


Figure E.3: Digitalised [17] and calculated heat conduction in comparison.

$$\lambda(T) = \left(1.76 \cdot 10^{-4} \frac{\text{W}}{\text{mK}^4} \cdot T^3 - 2.37 \cdot 10^{-1} \frac{\text{W}}{\text{mK}^3} \cdot T^2 + 79.5 \frac{\text{W}}{\text{mK}^2} \cdot T - 5.55 \cdot 10^3 \frac{\text{W}}{\text{mK}} \right) \cdot f_r$$

Reduction factor: $f_r = 0.8$

Table E.10: Radiation surface and finishing of components.

| Part | Surface [m^2] | Finishing | Note |
|----------------------|--------------------------|-------------------------|----------------|
| Chassis - top/bottom | $S_{Ch1} = 0.086$ | | for albedo |
| Chassis - side | $S_{Ch2} = 0.085$ | | for albedo |
| Chassis - total | $S_{Ch3} = 0.388$ | | for emissivity |
| Camera - housing | $S_{Cam} = 0.011$ | | |
| Camera - radiator | $S_{Rad} = 0.???$ | white paint | |
| Steer Engine | $S_{E,S} = 0.1$ | | |
| Drive Engine | $S_{E,D} = 0.04$ | | |
| Electric Bay | $S_{Bay} = 0.146$ | aluminium, sand blastet | |
| RTG | $S_{RTG} = 0.086$ | white paint | |

The cross sections were taken form the CAD model.

F Radiation

In this chapter, detailed calculations are performed on which Section 4.7 is based on. All calculations and figures in Section F are performed with SPENVIS unless otherwise stated. In order to simulate the radiation on Europa an orbit around Jupiter is simulated with the orbit parameters of Europa with a total mission duration of 30 days. The chosen parameters were an perijove altitude of 664,862 km, an apojove altitude of 676,938 km, and an inclination of 0.47°.

F.1 Jupiters Radiation Environment

In order to compare the radiation environment around Jupiter and the radiation environment around Earth the following trapped radiation models were used: for Jupiter the D&G83+Salammbo proton model and D&G83+GIRE+SalammboE electron model was used; for Earth the AP-8 proton model and the AE-8 electron model was used.

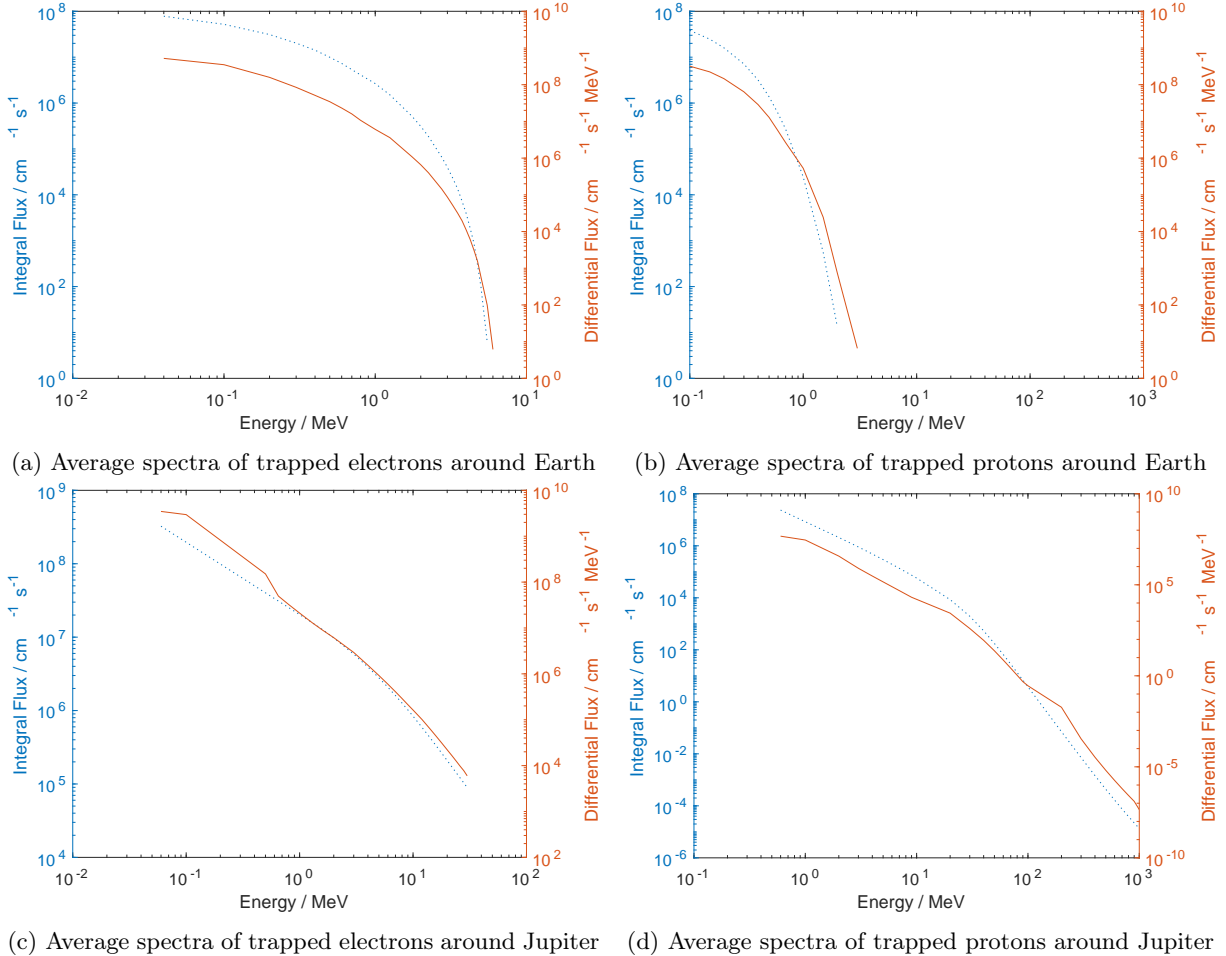


Figure F.1: Average trapped proton and electron fluxes on an orbit around earth at 25,000 km, through the outer Van Allen radiation belt, and on Europa's orbit around Jupiter.

F.2 Radiation Exposures

In order to simulate the TID for different radiation protections the Geant4 tool Multi-Layered Shielding Simulation (MULASSIS) is used. As target material silicon is selected with a thickness of $1 \mu\text{m}$. As shape a planar slab is selected because of the ice ground on one side of the rover.

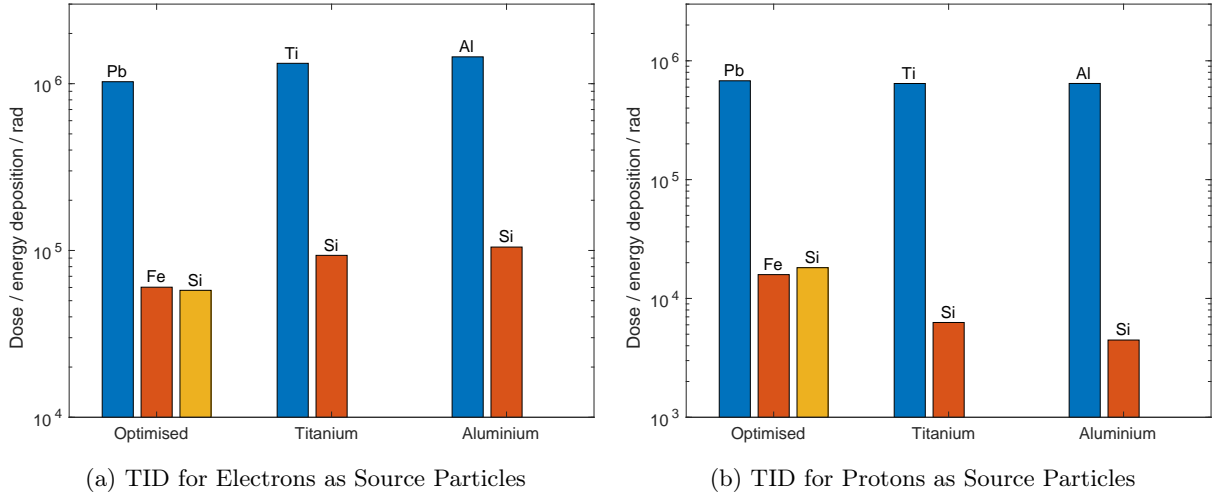


Figure F.2: TID of aluminium, titanium, and the optimised radiation structure shown in Table 4.7 with a weight target of all three structures of 0.5 g/cm^2 over 30 days of exposure on Europa.

Table F.1: Used components and the respective radiation tolerance and location

| Components | Rated TID | Exposed TID | Location |
|--------------------|-----------|-------------|--------------------|
| Electric Motors | - | < 205 krad | locomotion housing |
| Harness | - | < 98 krad | chassis |
| Stereo Vision Cams | 40 | < 31 krad | camera housing |
| OBC | 1000 | < 17 krad | E-Bay |
| PCDU | 20 | < 17 krad | E-Bay |

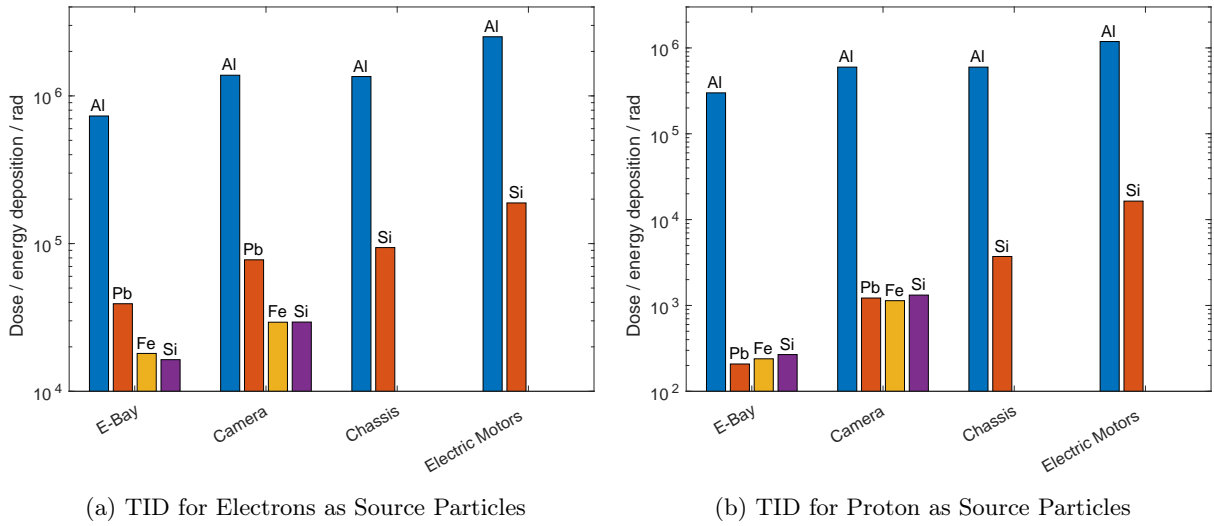


Figure F.3: TID for different compartments as seen in Figure 4.9. The E-Bay is shielded by 4 mm aluminium, 0.415 mm lead, and 0.033 mm iron; the camera compartment by 2 mm aluminium, 0.415 mm lead, and 0.033 mm iron; the chassis by 2 mm aluminium; the electric motors by 1 mm aluminium.

F.3 Improvements

All simulations of the improvements introduced in Subsection 4.7.3 are performed in the same way as in Subsection F.2.

In Figure F.4, the TID over 30 days within the E-Bay is shown. If all components with a radiation resistance under 43.27 krad are shielded individually, the additional shielding structure around the E-Bay can be removed and the aluminium structure would be sufficient.

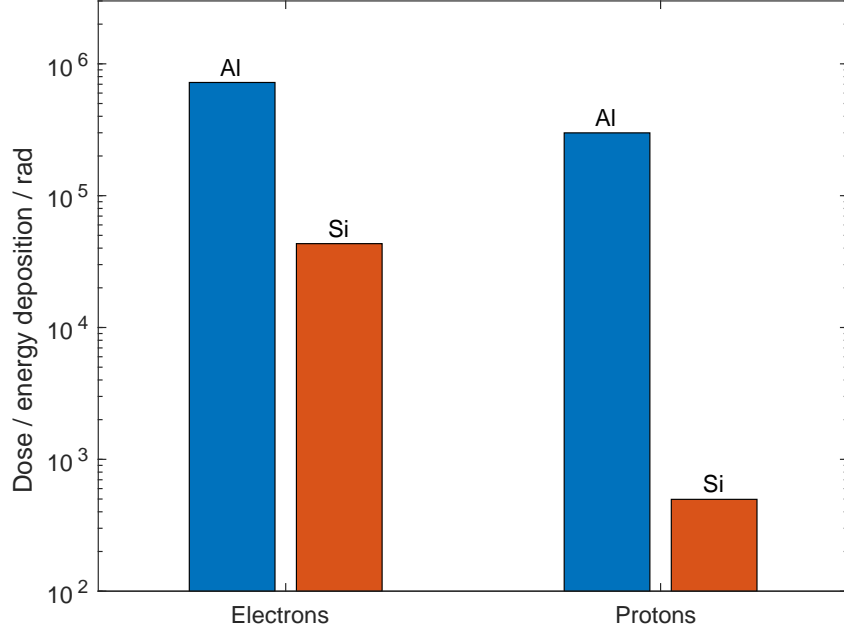


Figure F.4: TID with 4 mm Al shielding over a mission duration of 30 days

The resulting mass savings can be calculated with Equation 5.14 with m^* as the specific weight of the radiation protection and N as the amount of components within the E-Bay with a radiation resistance under 43.27 krad as of Table F.1.

$$\Delta m = SA_{E\text{-Bay}} \cdot m_{\text{Shielding}}^* - \sum_{n=0}^N SA_{\text{Component, n}} \cdot m_{\text{Shielding}}^* \quad (5.14)$$

With inserted values this results in a mass saving of $\Delta m = 736.2$ g.

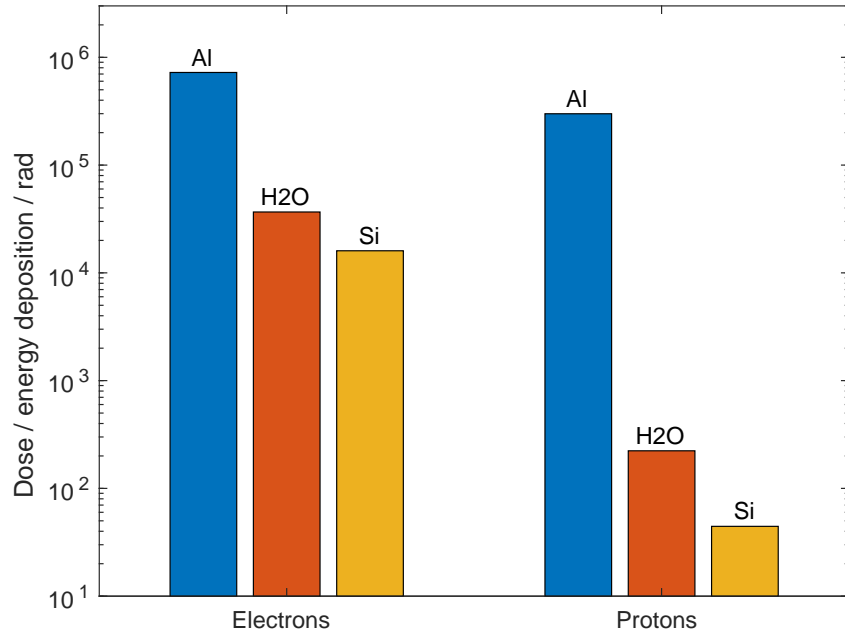


Figure F.5: TID with 4 mm Al shielding and 1 cm of Water over a mission duration of 30 days

G Digital Appendix